Continental Shelf Research 294 (2025) 105540

Contents lists available at ScienceDirect

Continental Shelf Research

journal homepage: www.elsevier.com/locate/csr

The role of barrier reef protection to storm surge during tropical cyclones in a narrow lagoon, New Caledonia, south west Pacific

Maxime Duphil [a,*], Jérôme Lefèvre [a], Swen Jullien [b], Jean Roger [c], Pascal Dumas [d], Romain Le Gendre [e], Jérôme Aucan [f], Myriam Vendé-Leclerc [g], Martin Bénébig [g], Christophe Menkes [a]

[a] Institut de Recherche pour le Développement, UMR 250 ENTROPIE (IRD, CNRS, Ifremer, Université de la Réunion, Université de la Nouvelle-Calédonie), BP A5, 98848, Nouméa, New Caledonia
[b] Université de Brest, Ifremer, CNRS, IRD, LOPS, F-29280, Plouzané, France
[c] The New Zealand Institute for Earth Science Ltd, 1 Fairway Drive, Lower Hutt, 5010, Aotearoa New Zealand
[d] Université de la Nouvelle-Calédonie, UMR 228 ESPACE-DEV, BP R4, 98851, Nouméa, New Caledonia
[e] Ifremer, UMR 250 ENTROPIE (IRD, CNRS, Ifremer, Université de la Réunion, Université de la Nouvelle-Calédonie), BP 32078, 98848, Nouméa, New Caledonia
[f] Pacific Community Center for Ocean Science (PCCOS), Pacific Community, BP D5, 98848, Nouméa, New Caledonia
[g] Service Géologique de Nouvelle Calédonie (SGNC), Direction de l'Industrie, des Mines et de l'Énergie de la Nouvelle Calédonie (DIMENC), BP M2, 98849, Nouméa, New Caledonia

ARTICLE INFO

Keywords:
Waves
Storm surge
Wave setup
Tropical cyclone
Coastal vulnerability
Barrier reef
Lagoon

ABSTRACT

Pacific islands are exposed to coastal hazards, particularly storm surges resulting from low pressure, extreme winds, and waves. While coral reefs naturally protect shorelines from incident waves, the diversity of reef geomorphologies induce various coastal responses, complicating hazard prediction based on offshore conditions. Understanding lagoon storm surge dynamics is therefore crucial for developing adaptation strategies to address global warming and sea-level rise. This study investigates the storm surge response of the narrow and shallow lagoon of Poe in New Caledonia using the SCHISM-SWAN coupled circulation-wave numerical model under tropical cyclone conditions. A retrospective of the 2019 cyclonic season shows that maximum storm surge is concentrated in the narrowest part of the lagoon, where human infrastructures are located, increasing exposure to extreme water levels. Modifying the reef structure to a more irregular form reveals that macro-scale reef features can mitigate wave setup intensity. Additionally, water depth variations over the reef crest significantly affect wave setup, with up to 30 % difference between high and low tides. A broader generalization based on 258 synthetic cyclone tracks highlights that within the lagoon, wave setup accounts for approximately 70 % of the storm surge, rising to 90 % during the most extreme event. These results show that the wave contribution is essential for accurate storm surge prediction. The findings provide critical insights for improving coastal hazard assessment, land use planning, and resilience strategies in reef island environments facing climate change.

1. Introduction

1.1. General settings about storm surge hazard and coral reef ecosystems

Global Mean Sea Level (MSL) rise poses a significant threat to low-lying coastal regions, especially small island states (Duvat et al., 2017; Li et al., 2019; Bremer et al., 2022). Since 1900, MSL has risen by ~0.2 m, with an accelerating trend, particularly in the Pacific region (IPCC et al., 2021; Nicholls and Cazenave, 2010). Sea Level Rise (SLR) exacerbates the frequency and severity of coastal flooding (Vitousek et al., 2017), often driven by storm surges, which result from the combined influence of atmospheric pressure anomalies (IBE), wind stress, and wave action (Idier et al., 2019). Extreme waves and induced wave setup are mainly triggered by extreme atmospheric events such as tropical cyclones (TCs) (Dietrich et al., 2011; Krien et al., 2017; Jullien et al., 2024) but they can also be generated by distant swell (Jullien et al., 2024; Hoeke et al., 2013; Ford et al., 2018). They may be exacerbated or damped by the phasing with the tidal cycle (Pedreros et al., 2018; Aucan et al., 2021), climate modes of variability (such as El Niño Southern Oscillation) (Jullien et al., 2024; Patra et al., 2020; Pagli et al., 2024)

* Corresponding author.
E-mail address: maxime.duphil@ird.fr (M. Duphil).

https://doi.org/10.1016/j.csr.2025.105540
Received 28 April 2025; Received in revised form 3 August 2025; Accepted 6 August 2025
Available online 7 August 2025
0278-4343/© 2025 The Authors. Published by Elsevier Ltd. This is an open access article under the CC BY license (http://creativecommons.org/licenses/by/4.0/).

and regional MSL variability associated to long-term trend (Vitousek et al., 2017). The severity of coastal impacts hence depends on the concomitance of sea level variations at various temporal scales. Along the shoreline, storm surges can induce three kinds of coastal submersions: overflowing (when the sea level rises until it overflows the shoreline), overtopping (when the sea level is unusually high and waves are overtopping the shoreline), and barrier breaching (when a natural or anthropic barrier is breached and water cross the shoreline), and each of them can follow one another during the whole storm surge episode (Chaumillon et al., 2017).

Natural ecosystems such as mangroves, seagrass, and coral reefs are known to play a mitigating role against ocean-induced flooding, notably by dissipating the waves energy and reducing propagation speed (Guannel et al., 2016). Human activities, on the other hand, can undermine the natural coastal protection provided by the ecosystem and play a key role in the risk (Duvat and Magnan, 2019). If man-made or grey infrastructures have been widely used so far (Klöck et al., 2022), nature-based solutions (NBS) have been suggested to help mitigate the growing risks (Storlazzi et al., 2018) and may be included in adaptation strategies to manage the storm surge risk at the local levels. Most scientific research on ecosystem services primarily takes an economic perspective with highly simplified assumptions (Barbier et al., 2011; Pascal et al., 2016). For example, global-scale estimates suggest that the annual economic damage from floods could double without coral reef protection, based on a breaker index and a 1-m reduction in reef top height (Beck et al., 2018). Such studies serve as tools for governments to develop coastal management strategies and adjust economic stakeholder policies. With the exception of specific studies (Reguero et al., 2021), the complexity and diversity of coral reefs and their associated ecosystems pose challenges in translating global economic projections to local scales. Effective risk reduction policies must be grounded in robust scientific knowledge of storm surges at appropriate spatial levels. Therefore, accurately assessing the mitigating role of these ecosystems requires high-resolution physical modeling that accounts for coastal geomorphology and dynamics, complemented by field observations.

In tropical islands with coral reefs, this ecosystem is the main geomorphological driver determining the natural protection capacity. Reefs are very effective at reducing incident wave impact by dissipating their energy through breaking and bottom friction. Defining a ratio between incident and transmitted wave heights across the reef (Ferrario et al., 2014), reported a range from 51 to 74 % of wave attenuation. On the other hand, wave forcing and dissipation induce changes in the mean water level, and advection of water across the reef (Symonds et al., 1995; Lowe et al., 2009; Sous et al., 2020a). Ultimately the resulting wave setup at the coast is thus difficult to predict, as it strongly depends on the reef geometry and lagoon geomorphology. Reef environments are generally classified as: fringing reef (reef connected to the coast by a shallow platform), barrier reef (reef separated from the coast by a wide lagoon), or reef-lagoon system (reef separated from the coast by a narrow lagoon).

In idealized shore, like a reef-lined coast, with normally incident waves (no gradient in quantities in the alongshore direction), the prediction of the steady cross-shore wave setup can be achieved using a 1D momentum balance equation (Eq. (1)) (Lowe et al., 2009; Sous et al., 2020a; Rijnsdorp et al., 2021).">

$$\underbrace{\rho_w g(\overline{\eta}+h)\frac{\partial \overline{\eta}}{\partial x}}_{\text{Pressure gradient (PG)}} = \underbrace{-\frac{\partial S_{xx}}{\partial x}}_{\text{Radiation stress gradient (RSG)}} + \underbrace{r_b}_{\text{Bottom stress (BF)}} - \underbrace{(\overline{\eta}+h)\frac{\partial \rho_w U^2}{\partial x}}_{\text{Advective acceleration (ADV)}} \quad (1)$$

in which x is the cross-shore axis, $\overline{\eta}$ the steady state component of the wave setup, U the depth-averaged velocity, ρ_w the water density, g the gravity acceleration, h the stillwater depth, S_{xx} the wave radiation stress (Longuet-Higgins, 1962) leading onshore flux of momentum as short waves break, and r_b which is the momentum sink due to bottom friction.

In coastally bounded reef systems free of channel (e.g fringing reef), the net cross-shore transport is nil, and Eq. (1) reduces to that used for sandy beaches (Apotsos et al., 2008a; Buckley et al., 2015; Martins et al., 2022) where pressure gradient is balanced by both radiant stress gradient and bottom friction in the surf zone. There, wave setup has been shown to play a key role in coastal erosion and flooding (Cuttler et al., 2018). In barrier reef environments, the coastal storm surge depends on a more complex balance between wave setup and wave-induced flow over the barrier. As this water moves across rough over the reef top, it experiences significant frictional resistance leads to head loss which induce onshore-directed flow resulting in a setdown on the back reef (Sous et al., 2020b; Zhu et al., 2024). In the reef-lagoon system, the piling-up of water in the coastally bounded lagoon driven by onshore-directed currents implies the development of return flow outside the lagoon through channels and gaps in the barrier reef. There, the wave setup is exacerbated owing to enhanced frictional resistance on the return flow over the reef and shallow and/or narrow channels (Lowe et al., 2009; Taebi et al., 2012). In contrast to the fringing-reef case, the nonzero cross-reef net transport, the wave-induced lagoon circulation and changes in depth at transition with channels implies that advection contribute also in Eq. (1), as detailed in (Rijnsdorp et al., 2021).

The wave setup dynamics is constrained by multiple local factors regarding reef-lagoon details (cross-reef shape, roughness, opening of channels, reef submergence depth, lagoon width and depth, etc.) as investigated in 1D scenario by (Lowe et al., 2009; Zhu et al., 2024; Buckley et al., 2016), as well as their interplay with other forcing factors, like changes in MSL due to tide (Becker et al., 2014) and the horizontal lagoon circulation, modified by wave-driven flows (Yao et al., 2018). Smooth or abrupt changes in the reef slope such as submarine canyon (Apotsos et al., 2008b) or indentations in the shape of the barrier reef (Mandlier, 2013) exert a fundamental control on the incident wave field. This leads to differences in how wave energy is distributed along the shoreline, creating spatial variations in the wave forces. As a result, it becomes more difficult to accurately predict wave-induced water levels and current patterns in the areas behind the reef.

The accurate evaluation of extreme coastal storm surge in realistic complex coastal morphologies therefore strongly depends on incident wave conditions, wave transformation (Pomeroy et al., 2012; Sous et al., 2019; Bertin et al., 2025), wave-current interactions (Guérin et al., 2018; Jullien et al., 2020; Ye et al., 2020) and wave dissipation by bottom friction (Rijnsdorp et al., 2021; Buckley et al., 2016; Pezerat et al., 2021). Although important progress has been achieved over the last decade regarding the understanding and modeling of such processes, every reef-lagoon has its unique geomorphology, and only a few studies have been conducted under extreme events, questioning the generic nature of previous findings.

1.2. Application to our study site in New Caledonia lagoons

New Caledonia is a French Archipelago located in the southwestern Pacific Ocean just ~100 km north of the tropic of Capricorn, about 1400 km east of Australia and 1600 km north of New Zealand (Fig. 1A). New Caledonia is surrounded by one of the longest barrier reefs in the world and offers a large geomorphological lagoon diversity (Andrefouët and Wantiez, 2010). Their shapes go from very wide (>40 km) and deep (>25 m) lagoons opened by numerous channels, to narrow (<1 km), shallow (<2 m) and semi-enclosed ones. These lagoons also host numerous islets (>140), some of them being inhabited. New Caledonia reefs and lagoons are internationally recognized for their outstanding high diversity of habitats, variety of life, and general good health (Pelletier et al., 2024). They were declared a UNESCO World Heritage site in 2008 (Payri et al., 2019). Because of its oceanic location, New Caledonia is exposed to different types of marine submersion linked to extreme geological events such as tsunamis (Roger et al., 2019, 2021),

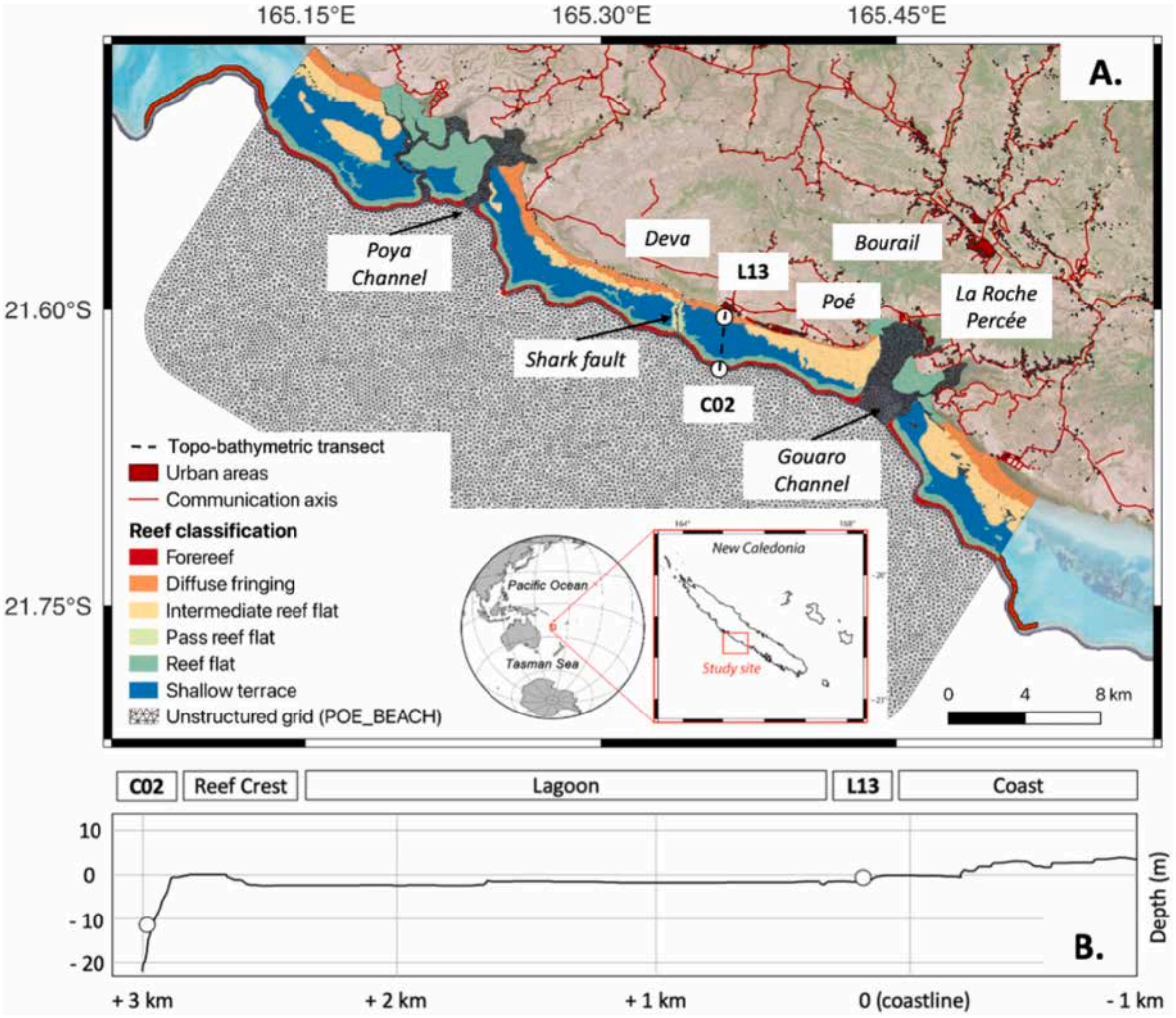

Fig. 1. Map of the Poe lagoon (A) and coastal area located on the west coast of New Caledonia (see insert). Urban and touristic areas (Bourail, La Roche Percée, Poé, Deva) are colored in dark red, as well as communication axes. The lagoon reef types are shaded in colors (see legend). The lagoon outflows areas are pointed (Poya Channel, Shark fault, Gouaro Channel). The unstructured model grid of one Poe configuration is represented. The location of two in-situ pressure sensors is indicated: L13 located in front of a tourist resort at 2 m depth, and C02 located on the forereef at 11 m depth. Topo-bathymetric profile in the model between both L13 and C02 stations is indicated to highlight the very shallow water depth in the lagoon and the low-lying coastal strip (B).

and meteorological events like tropical and extratropical storms and cyclones (Jullien et al., 2024). The local wave climate is characterized by south swells coming from the Tasman Sea and the Southern Ocean, southeasterly waves generated by the trade winds and more episodic swells generated in the northern hemisphere off Japan (Pagli et al., 2024). During the cyclonic season extending from December to May, episodes of extreme waves induced by tropical cyclones are also observed with ~3.5 cyclones per year (Diamond et al., 2013) recorded in the Economic Exclusive Zone (EEZ).

The present study focuses on the case of the narrow and shallow lagoon located off Poe, a coastal settlement on the central west coast of Grande Terre (Fig. 1A). Poe lagoon is geomorphologically unconventional in the general Caledonian lagoon landscape, with a 30 km-long coral barrier reef, almost continuous, with 70 % oriented from N-W (315°) to S-E (135°) direction parallel to the coast. The sinuosity of the barrier reef is very pronounced, adding 10 % more reef length than a straight linear structure. The average distance between the reef and the coastline is approximately 2 km, ranging from a minimum of 1.7 km to a maximum of 3.7 km (Fig. 1A and B). The mean reef crest is 1 m high over the barrier but varies along the reef showing several dead-end passages. This lagoon has the advantage of being at the same time almost "idealized" in its shape with few openings to the ocean: the 600 m wide Poya Channel on the northern edge, the 1800 m wide Gouaro Channel on the southern edge, and the narrow 100 m wide Shark Fault at the center (Fig. 1A), and characterized by a wide diversity of coastal ecosystems (patches of mangrove, seagrass meadows, scattered reefs, sandy and reef flats, reef barrier; for more details see (Andrefouët et al., 2006) and Fig. 1A). The area has been protected since 1993 for conservation purposes of its great faunistic and floristic biodiversity, such as the coral reefs and associated ecosystems, and is classified as a natural reserve within the West Coast Provincial Park (https://www.province-sud.nc/pandoreweb/app/aireProtegee/PZCO). This area has been subjected to scientific monitoring by Ifremer (Institut français de recherche pour l'exploitation de la mer) studying the green algae bloom events in 2018 (Brisset et al., 2021) and several field surveys have been conducted aiming at better understanding the hydrodynamic behavior of the lagoon (Bruyère et al., 2022; Lalau et al., 2022). In New Caledonia, the tidal cycle is semi-diurnal with a range reaching a maximum of 1.80 m according to observations in Gouaro bay during 159 days (SHOM). Poe lagoon is also of particular interest regarding coastal vulnerability issues, as its coastal zone is characterized by a low-elevated coastal zone (LECZ) (<5 m) where human activities are quite developed at less than 100 m from the coastline (urban areas of the village of La Roche Percée and Poe, resorts, campgrounds, recreational tourism activities, see

Fig. 1A). Poe lagoon experienced strong storm surges during two recent TC events. Poe lagoon was one of the most impacted areas with a strong wave setup (Jullien et al., 2020) such as Cook TC (2017). In 2019, Oma TC passed offshore of the New Caledonia West coast, generating strong waves that induced an observed storm surge of more than 0.8 m (see more details in Section 3).

That lagoon setting is scrutinized to address its ecosystem mitigating role. Series of experiments are conducted to document the coastal hazards for storm surge risk management in New Caledonia. Relying on the development of a 2D coupled wave-current numerical model, and taking advantage of recently surveyed data in the lagoon (Section 2), we first investigate storm surge processes, in particular those driving the wave setup, and its sensitivity to the lagoon geomorphology during a tropical cyclone (Section 3). In order to generalize storm surge assessment under tropical cyclones, we further characterized its coastal distribution and the relative wave contribution for a set of 258 statistically-generated synthetic tropical cyclones, and we quantify the impact of such hazards on the coastal vulnerability. In Section 4, we discuss the limits of our modeling approach, the results in comparison with other reef-lagoon systems by the relevance of empirical or semi-analytical formulations to predict the wave setup and the climate change implications for the mitigating role of coral reefs in such a lagoon system.

2. Material & methods

2.1. In-situ observations

A field survey was conducted in Poe lagoon by Ifremer from the 5th of February to the May 7, 2019 (~4 months) to monitor water level variations including tides and incident waves (Bruyère et al., 2022). Bottom pressure sensors (RBR Duo/Duet 2.0) continuously recording pressure at a sampling rate of 1 Hz were deployed at 11 m depth on the forereef (C02, Fig. 1) and at 2 m depth inside the lagoon (L13, Fig. 1). From the pressure records and by assuming hydrostatic pressure, hourly averaged total water depths $(\eta+h)$ are derived at both stations. Following the approaches of (Lowe et al., 2009; Sous et al., 2020a; Pezerat et al., 2021), the mean water level variability $(\overline{\eta})$ is expressed relative to the deepest pressure sensor:

$$\overline{\eta} = (\eta + h)_{L13} - (\eta + h)_{CO2} + (h_{mean(CO2)} - h_{mean(L13)}) - (A_{(L13)} - A_{(CO2)}) \quad (2)$$

In Eq. (2), the third term $(h_{mean(C02)} - h_{mean(L13)})$ is a correction using the mean water depths (e.g 10.86 m 2.26 m respectively) to express $\overline{\eta}$ as relative to the still water level. Nevertheless $\overline{\eta}$ is driven by changes in wave setup and tides. Usually, tidal elevations are approximated as similar at all stations, and the first three terms are expected enough to remove both the tidal and low-frequency sea level variations (Monismith et al., 2013). By computing tidal harmonic constants and by a close inspection of the computed anomaly between the predicted astronomical tide at stations C02 and L13 (not shown), noted $A_{(C02)}$ and $A_{(L13)}$ respectively, it was evidenced that the shallow and elongated lagoon of Poe is not free of tidal deformation. Such deformation is characterized by a phase lag of about 15 min and generation of M2 (semi-diurnal) overtides. To reduce the effect of tidal deformation by the lagoon, a second time-varying correction [−0.2–0.2 m] is applied on Eq. (2). From Eq. (2), the IBE is canceled, and $\overline{\eta}$ is defined as the super-elevation of the lagoon due to the wind-stress, wave breaking and possible nonlinear effects between tides and the wave-driven circulation.

Wave parameters are evaluated from the pressure sensor data using a Fourier transform to obtain a pressure spectrum, then the linear wave theory is applied. A fixed cutoff frequency to separate sea-swell (SS) and infragravity (IG) waves may blur the distinction between energy bands, but this threshold is consistent with prior studies in similar reef-lagoon environments (Van Dongeren et al., 2013; Aucan et al., 2017; Locatelli et al., 2017) and is appropriate for swell-dominated settings such as Poe lagoon. A 0.04 Hz cutoff was applied to filter out IG and very low-frequency waves, which were not addressed in this study. To validate this choice, the spectral energy distribution at station L13 was analyzed using frequency-domain method across the entire observation period, including ±48 h and ±6 h around the Oma TC peak. The results consistently showed that the 0.04 Hz cutoff clearly separated IG and SS energy bands. During the peak of Oma TC (25th of February), wave energy at L13 was dominated by the short-wave (SW) band (70 %), followed by SS (27 %) and IG (3 %). These results indicate that IG played only a minor role at the TC peak relative to short-period waves. Overall, the selected threshold remains well supported by the literature and the spectral characteristics observed in this study, despite the inherent limitations of a fixed cutoff frequency.

2.2. The modeling system

The dynamics of the reef-lagoon system is modeled with a 2D wave-current coupled system using the Simulating WAves Nearshore phase-averaged model (SWAN, version 41.2 (Booij et al., 2004),) coupled with the Semi-Implicit Cross-scale Hydrosciences Integrated System Model (SCHISM, version 5.7 (Zhang et al., 2016),) in its 2D vertically integrated version. Coupling between waves and currents is performed, as in past works (Dodet et al., 2013), by providing the surface forcing, water levels and ambient currents from SCHISM to SWAN, and by incorporating the wave effects on the circulation in SCHISM using wave parameters computed in SWAN (see details in Section 2.2.2). The variables are exchanged from one model to another every 5-time steps of 60 s. Both SCHISM and SWAN use the same unstructured grid for each experiment which is presented in Section 2.3.

2.2.1. Wave model: SWAN

SWAN simulates the wave generation by the wind, refraction due to currents and depth, non-linear interactions between waves, bottom friction and depth-induced breaking, transmission through and reflection from obstacles, and diffraction. Wind waves are represented by the wave action density spectrum, $N(\sigma,\Theta)$, with σ and Θ the relative angular frequency (from 0.031 to 1.42 Hz) and the direction of wave propagation (with 36 discrete directions) respectively. In our implementation, SWAN employs the Strongly Implicit Procedure (SIP) scheme, to solve the spectral wave action balance, which is robust in shallow waters using unstructured mesh with complex topography (http://www.swan.tudelft.nl). The numerical propagation scheme is based on a four-direction Gauss-Seidel iteration technique. Physics, based on the linear wave theory, numerical schemes and their limitations are explained in (Booij et al., 2004; Zijlema, 2010). In this study, physics from (Snyder et al., 1981; Komen et al., 1984) are used for the energy transfer from wind to wave, while formulation by (Komen et al., 1994) is applied for dissipation by whitecapping. Energy dissipation due to bottom friction and depth-induced breaking follows physics from (Madsen, 1994) using a constant roughness length scale of 0.05 and from (Battjes and Janssen, 1978), with a breaker index of 0.73 respectively.

2.2.2. Hydrodynamic model: SCHISM

SCHISM solves the 3D Reynolds-Averaged Navier-Stokes (RANS) equations using a semi-implicit finite-element and finite-volume method on unstructured grids (Zhang et al., 2016) with time stepping with no Courant–Friedrichs–Lewy (CFL) stability/convergence condition. The model has been widely used to study the general circulation (Yu et al., 2017), tsunamis (Roger et al., 2021; Zhang et al., 2011), and also marine flooding (Krien et al., 2017b; Bertin et al., 2014). In 2D, RANS equations are depth-integrated, and the circulation is described using Non-linear Shallow-water Wave (NSW) equations (see Eqs. (3) and (4)):

$$\frac{\partial \eta}{\partial t} + \nabla . H\boldsymbol{u} = 0 \quad (3)$$

$$\frac{\partial \boldsymbol{u}}{\partial t}+\boldsymbol{u}.\nabla\boldsymbol{u}=-g\nabla\left(\eta+\frac{P_s}{g\rho}\right)+f(\boldsymbol{v},-\boldsymbol{u})+\boldsymbol{F_{wv}}+\frac{\boldsymbol{\tau_s}}{\rho_w H}-\frac{\boldsymbol{\tau_b}}{\rho_w H}+\frac{\upsilon}{H}\nabla.\nabla(\boldsymbol{u}H) \quad (4)$$

where u, v represents the horizontal velocity components, H the total depth $(\eta + h)$, P_s the atmospheric pressure at the surface, f the Coriolis parameter, τ_s the surface stress due to wind, F_{wv} the wave force due to radiation stress gradients (RSG, see Eq. (1)), and the last term the resistance due to horizontal eddy viscosity (with υ set constant in time, $10^{-6} m^2.s^{-1}$). Vector quantities are in bold. The wind shear stress τ_s is parameterized using the approach of (Zijlema et al., 2012). The bottom stress τ_b involved in the BF term (Eq. (1)) is computed using a logarithm friction law with a background apparent roughness of 3 mm. The roughness value is updated to include wave effects on the bottom boundary layer using a modified Grant-Madsen formulation (Zhang et al., 2004) at each time step of the wave model.

As detailed in (Dietrich et al., 2011), the Longuet-Higgins formalism is applied to derive the two components of F_{wv} (see Eqs. (5) and (6)) using cross-shore (S_{xx}), along-shore (S_{xy}) and diagonal (S_{yy}) components of the radiation stress tensor (Buckley et al., 2015):

$$F_{wv,x} = -\frac{\partial S_{xx}}{\partial x}-\frac{\partial S_{xy}}{\partial y} \quad (5)$$

$$F_{wv,y} = -\frac{\partial S_{xy}}{\partial x}-\frac{\partial S_{yy}}{\partial y} \quad (6)$$

$$S_{xx}=\rho g\iint\frac{E}{2}\left(2\frac{C_g}{C}\left(cos^2\,\theta+1\right)-1\right)d\sigma d\theta \quad (7)$$

$$S_{xy}=\rho g\iint E\frac{C_g}{C}sin\,\theta\,cos\,\theta\,d\sigma d\theta \quad (8)$$

$$S_{yy}=\rho g\iint\frac{E}{2}\left(2\frac{C_g}{C}\left(sin^2\,\theta+1\right)-1\right) \quad (9)$$

In Eqs. (7)–(9), E is the wave energy density, $\frac{C_g}{C}$ represents the ratio of

Table 1
Summary of numerical model experiments. Simulations used for validation with in-situ data are in orange. Simulations used for sensitivity tests with Oma TC in the first set of experiments are in blue. Simulations used for the generalization of storm surge with synthetic TCs in the second set of experiments are in green. Depth values [m] are vertically referenced to local hydrographic Chart Datum (SHOM).

Grid name	Acronym	Resolution	Bathymetry	Forcing
POE_BEACH	REF	250 - 30	DEM if >15m Landsat-8 if <15m and >2m Sentinel-2 if <2m	Atm: AROME Oce: Mercator + TPXO Waves: MFWAM
	REF_NOWAVE	250 - 30	DEM if >15m Landsat-8 if <15m and >2m Sentinel-2 if <2m	Atm: AROME Oce: Mercator + TPXO No wave coupling
	LOWBAT	250 - 30	DEM	Atm: AROME Oce: Mercator + TPXO Waves: MFWAM
	CR005	250 - 30	DEM if >15m Landsat-8 if <15m and >2m Sentinel-2 if <2m Reef crest = 0.05m	Atm: AROME Oce: Mercator + TPXO Waves: MFWAM
	CR100	250 - 30	DEM if >15m Landsat-8 if <15m and >2m Sentinel-2 if <2m Reef crest = 1.00m	Atm: AROME Oce: Mercator + TPXO Waves: MFWAM
	IDEAL_S	250 - 30	Average REF bathymetry integrated along cross-shore normal Reef crest = 1.00m	No atmo. forcing Oce: Synthetic tide Waves: Parametric
	IDEAL_W	250 - 30	Average REF bathymetry integrated along cross-shore normal Reef crest = 1.00m	No atmo. forcing Oce: Synthetic tide Waves: Parametric
NC_BOX	LOWRES	2500 - 70	DEM	Atm: AROME Oce: Mercator + TPXO Waves: MFWAM
	STATTC_NOWAVE	2500 - 70	DEM	Atm: Synthetic TCs Oce: Mercator + TPXO No wave coupling
	STATTC	2500 - 70	DEM	Atm: Synthetic TCs Oce: Mercator

group celerity and wave celerity and θ represents the angle of incidence computed as the mean wave direction. From Eqs. (7)–(9), it is worth noting that under normally incident waves ($sin\,\theta = 0$) and for uniform alongshore settings like considered in Eq. (1), the contribution of both S_{xy} and S_{yy} vanishes and that only the gradient of S_{xx} in the cross-shore direction is the main player explaining the increase of $\overline{\eta}$ at the coast.

2.3. Numerical experiments

Two computational domains using SCHISM-SWAN are used in the present study (Table 1). The first high-resolution configuration focuses on the Poe lagoon (named POE_BEACH). It is designed to address the storm surge sensitivity to the reef-lagoon geomorphology. The second configuration covers a larger regional domain (named NC_BOX). It is designed to generalize storm surge hazards in Poe lagoon by using a large range of cyclonic forcings applied on a regional grid, which is less computationally intensive, and encompasses more largely the TC tracks.

2.3.1. High-resolution POE_BEACH experiments

The POE_BEACH grid includes 33 000 nodes. The horizontal mesh resolution ranges from 250 m in the open deep-ocean to 30 m along the coastline and the barrier reef (see bathymetric grid in Appendice A). Seven simulations are performed on this grid over the observed period from February to May 2019. The reference simulation (REF), considered as the most realistic one, uses the Satellite Derived Bathymetry (SDB) from Sentinel-2 for shallow bathymetry (<2 m) of (Amrari et al., 2021) and from Landsat-8 for depth until 15 m. Bathymetry from the New Caledonia DEM (https://doi.org/10.17183/MNT_NC100m_TSUCAL_WGS84) was used for depths >15 m. Hourly surface forcing such as wind and pressure is imposed using outputs from Météo-France in regional weather forecast model (named AROME (Faure et al., 2020),) at 2.5 × 2.5 km spatial resolution (https://donneespubliques.meteofrance.fr/?fond=produit&id_produit=241&id_rubrique=51). Along the ocean boundaries, 6-hourly outputs for currents and water level from the Mercator-Ocean NEMO (Nucleus for European Modeling of the Ocean) global 1/12° reanalysis (https://doi.org/10.48670/moi-00021) are imposed. The tide variability is accounted for by adding tide information (elevation and currents) from the Oregon State University Topex/Poseidon product (TPXO7) (Egbert and Erofeeva, 2002). Along the open boundaries of the wave model, a wave spectrum is applied using information from the French Weather Agency wave model (MFWAM) reanalysis (https://doi.org/10.48670/moi-00017). In that product, wave parameters (significant wave height, H_s, period and direction of the peak, T_p and D_p) for one wind-sea partition and the two most energetic swell partitions are provided every 3-h on a 30 × 30 km spatial resolution grid.

A twin simulation with no wave coupling (REF_NOWAVE) is conducted to assess the wave contribution ($\overline{\eta}_{wav}$) to the storm surge by subtracting REF_NOWAVE from the coupled current-wave REF simulation. Then several sensitivity experiments are conducted to evaluate the impact of the reef shape, bathymetry and reef crest height on the reef-lagoon dynamics. They are summarized in Table 1, and described in the following.

It is worth noting that the Poe lagoon system is characterized by a nearly straight reef in the southern part and a more undulating reef in the northern part (Fig. 1), with a succession of shallow platforms and canyons extending out from those barrier reef features (not shown), having a potential to focus or diverge the wave energy after wave refraction at the reef. To explore wave-induced dynamics due to macro-scale variations in the reef shape, two idealized experiments using contrasted reef-lined settings are conducted. The first idealized simulation features a straight reef-lined coast (IDEAL_S) where the barrier reef is aligned at a distance of 2.5 km from the coastline. To mimic a uniform alongshore setting between Gouaro and Poya channels, a cross-shore depth profile is constructed using the mean bathymetry from REF. As a result, the linear barrier reef has a forereef slope of 1/25 with a uniform height of the reef crest of 1.00 m (Table 1). The second idealized simulation features an undulating reef (IDEAL_W) using a sine curve with a wavelength of 4 km and an amplitude of 600 m to mimic the undulating reef present in the northern part of Poe lagoon.

These idealized simulations are performed during 1-month long with constant air pressure, a sea level variability imposed using the M2 tide (period of 12.42 h and amplitude of 0.8 m), without wind, earth rotation turned off ($f(v, -u) = 0$ in Eq. (4)), and using stationary and normal-to-the-reef incident waves imposed with a JONSWAP (Joint North Sea Wave Project (Hasselmann et al., 1973),) spectrum corresponding to the peak of Oma TC ($H_s = 7$ m, $T_p = 11$ s, $D_p = 6°$ relative to the cross-shore direction) on the February 25, 2019. Changes in the wave-induced dynamics and wave setup due to macro-scale variations in the reef shape is then evaluated through the analysis of the mean momentum balance (Eq. (1)). The comparison of the momentum terms and the expected balance between them in the cross-shore direction requires a uniform topography in the alongshore direction (Gourlay, 1996) which is respected in our idealized IDEAL_S setting, but weakly satisfied in IDEAL_W.

Three additional realistic sensitivity simulations are performed keeping the same forcings as REF. The first one (referred to as LOWBAT), assessing the impact of the bathymetry, uses the New Caledonia DEM (https://dx.doi.org/10.17183/MNT_NC100m_TSUCAL_WGS84), which has a coarser resolution of 100 m compared to that used in REF, while keeping the same mesh resolution. This implies a reduction in water depth of ~1.0 m within the lagoon. Two other simulations are conducted to assess the impact of the reef crest height on the lagoon hydrodynamics with the same bathymetry as REF, but modifying the reef crest height to uniform depths of 1.0 m (CR100 experiment) and 0.05 m (CR005 experiment) in accordance with the literature (Hoeke et al., 2013; Buckley et al., 2016; Storlazzi et al., 2004; Huang et al., 2012). In these experiments, the reef crest is considered as a buffer zone over the barrier reef straddling the shallowest part of the forereef and the beginning of the reef flat (see reef classification from (Andrefouët et al., 2006)).

It is worth noting that, to infer $\overline{\eta}$ and compare it with observations, the same methodology detailed in Section 2.1 (Eq. (2)) is applied to model outputs at the closest model point to the in-situ lagoon stations by subtracting from offshore modeled sea level.

2.3.2. Regional NC_BOX experiments

The second set of experiments aims to assess extreme storm surge using a collection of tropical cyclones. It was conducted using a coarser regional unstructured grid (NC_BOX) that is more suitable in representing TC wind forcings in both the near- and far-field given its larger domain. In NC_BOX, the grid has a total of 320 000 nodes, encompassing the whole New Caledonia archipelago with the following spatial extent: [160°E−170°E] and [25.5°S-16°S] (see bathymetric grid in Appendice A). Mesh generation and bathymetry from DEM of New Caledonia are similar with those detailed in (Roger et al., 2021). All New Caledonia lagoons are represented with lower spatial resolution ranging from 2.5 km to 70.0 m at the coast. Several experiments are designed (summarized in Table 1) for NC_BOX. First, using similar meteo-oceanic forcing as those detailed in REF, the LOWRES simulation is conducted to investigate the performance of this larger-scale configuration in the Poe lagoon, and investigate the impact of the model grid resolution by comparing LOWRES and LOWBAT.

Then, a set of simulations is performed to generalize the storm surge response in Poe lagoon, using a collection of synthetic storm tracks driving waves and circulation in NC_BOX. Toward that end an ensemble of 4210 synthetic cyclone tracks and intensities were generated with the STORM package (Bloemendaal et al., 2020) over the NC_BOX region. Among these, a subset of 258 TCs is chosen to simulate storm surge with and without wave coupling (respectively STATTC and STATTC_NOWAVE experiments), to understand the contribution of waves by

isolating the quantity $\overline{\eta}_{wav}$ which is computed by subtracting STATTC_NOWAVE from STATTC sea level. This subset was extracted to maximize the diversity of statistical synthetic storm tracks in terms of intensity, structure of surface wind and pressure and track. The Parametric Hurricane Model (PaHM, https://github.com/noaa-ocs-modeling/PaHM), implemented as a module in SCHISM, was used to derive 10-m wind and surface pressure forcings over the NC_BOX grid using the 3-hourly time series of storm parameters (e.g location and maximum wind speed) generated from STORM. The parametric hurricane vortex model used was the Generalized Asymmetric Vortex Model (GAHM) developed by (Gao et al., 2013). In both STATTC and STATTC_NOWAVE, and for all storms, the ocean model is initialized from a solution resulting from a 10-days spin up simulation running with no wind and no wave-induced forcing, a surface pressure equal to 1013 hPa, and lateral boundary conditions derived from Mercator-Ocean NEMO global 1/12° reanalysis on January 1st, 2020 and a constant sea level anomaly that mimics high tide (+1.6 m relative to local chart datum from SHOM). Storm surges are computed from STATTC by subtracting sea level from a reference simulation running without PaHM forcing.

3. Results

3.1. Numerical validation during the observed period

During the observed period in 2019, a tropical depression named Oma formed to the North of New Caledonia on February 11th and evolved to a TC on February 20th at [161°40E, −21°10S] (https://www.meteo.nc/8-actualites/534-bilan-du-passage-du-cyclone-tropical-oma-du-11-au-26-fevrier-2019#bilan-des-precipitations). It crossed the New Caledonia region twice with an unusual path. First on February 19th while moving on a southward path and second on the 25th when moving back towards New Caledonia from the south. At the closest meteorological station to Poe (Tontouta, Météo France), the minimum recorded atmospheric pressure was 996 hPa on February 20th and 1002 hPa on February 26th. It is well represented by the AROME forcing (see Appendice B1). In New Caledonia, this cyclonic event was not considered to have major terrestrial impacts as winds and rainfall were not very high on land. At historical tide gauge stations on Grande Terre and the Loyalty Islands, storm surges typically averaged around 30 cm, varying by event (Duphil, 2024). In-situ data revealed that narrow lagoons, such as Poe, are particularly sensitive to storm surge, illustrated by the increase of $\overline{\eta}$ (Eq. (2)) during Oma TC (83 cm at the lagoon L13 station in February 25th and more than 60 cm during two consecutive days, Fig. 2). It is worth noting that when the storm made landfall, the IBE triggers a small increase of the sea level of about 10 cm (not shown), not reproduced in the evolution of $\overline{\eta}$ (Fig. 2), since changes in atmospheric pressure in both stations offset each other in Eq. (2). For the remainder of the analysis on Oma TC, we treat $\overline{\eta}$ as a proxy for storm surge, given that IBE is neglected in the lagoon wave setup.

During Oma TC, initial easterly winds (~65 kts) shifted to southwesterlies (~30 kts) (see Appendice B1), generating significant offshore swell ($H_s > 6$ m) from SW (see Appendice B2), slightly below the ~7 m observed on the forereef (Fig. 2A–C). No other storms occurred during the study period. Both fine (REF) and coarse (LOWRES) simulations reproduced the phase and amplitude of observed H_s at station C02 (REF: RMSE = 0.29 m, R^2 = 0.83; LOWRES: RMSE = 0.32 m, R^2 = 0.86, Fig. 2A), although both underestimated the peak by ~2 m, likely due to limitations in wind forcing (see Appendice B1) and wave boundary conditions (see Appendice B2). The MFWAM product itself had an RMSE of 0.556 m and R^2 of 0.858, capping H_s at 6 m, which suggests a slight underestimation of extreme offshore waves, also notify in (Gaffet et al., 2025).

At station L13, storm surge was also well reproduced (REF: RMSE = 8.5 cm, R^2 = 0.64; LOWRES: RMSE = 9.1 cm, R^2 = 0.58, Fig. 2B). But during Oma TC, water levels remain abnormally elevated for several tidal cycles, up to two days. A first storm surge peak was slightly underestimated (~19 cm for REF, ~6 cm for LOWRES, Fig. 2D), while a second peak is missed in both REF and LOWRES simulations. This may result from slightly underpowered MFWAM wave forcing and imperfect TC translation speed, leading to a short-lived lagoon storm surge. Additionally, despite higher-resolution bathymetry in REF, incomplete or inaccurate data in the narrow channels may affected the modeled surge-driven outflow dynamics (see Section 3.2). Overall, these results give confidence in using our 2D model configuration, enabling a more detailed study of the physical processes influencing extreme storm surge in Poe lagoon.

3.2. Processes driving storm surge within the lagoon

In the following, we study changes in $\overline{\eta}$ investigated through storm surge along the coast induced by Oma TC and its sensitivity to the reef-lagoon configuration. The aim is to identify the geomorphological parameters playing a key role in the pattern and intensity of storm surge.

Fig. 3 first presents the duration and spatial distribution of storm

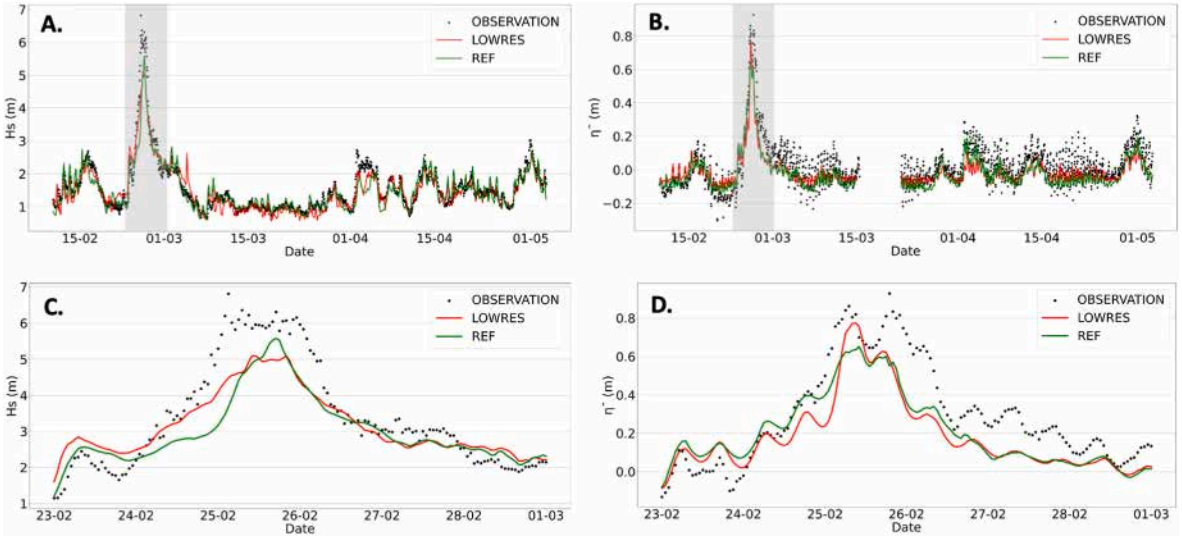

Fig. 2. Time series of H_s [m] at the C02 forereef station (panels A, C) and $\overline{\eta}$ [m] at L13 nearshore lagoon station (panels B, D). Panels C and D are respective zooms of panels A and B (in grey) during the Oma TC peak which corresponds to 25th of February 2019. The in-situ observations are displayed in black; simulation REF is shown in green and LOWRES in red.

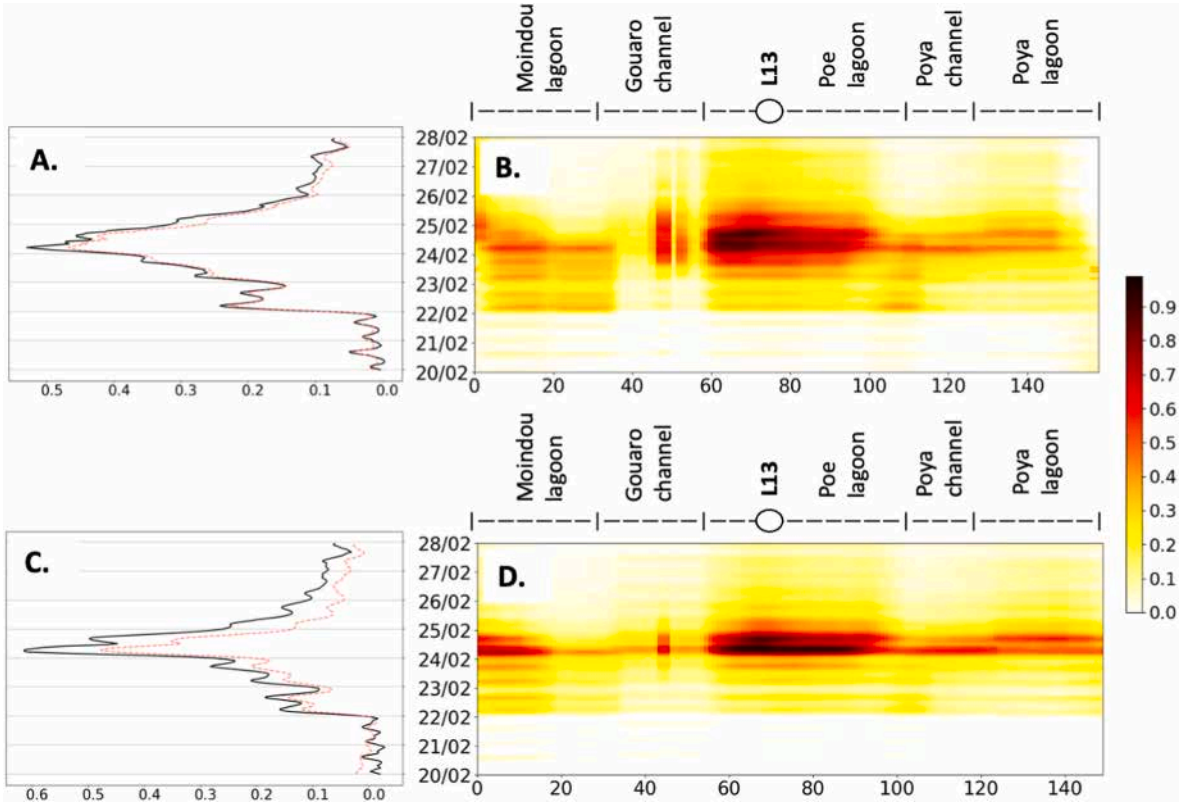

Fig. 3. Time series of mean coastal $\overline{\eta}$ in black [m] and $\overline{\eta}_{wav}$ contribution in red [m] for REF and LOWRES configuration (panels A, C). Hovmöller diagrams of $\overline{\eta}$ [m] uniformly extracted along the shoreline (with dx = 100 m) for the both configurations (panels B, D) during Oma TC (10 days). Lagoons and channels are marked by coastal segments including L13 station position in bold. Sea level changes along the coast are referenced to the offshore station O2, as detailed in Eq. (2).

surge along the coastline (Fig. 3B–D), as well as the contribution of $\overline{\eta}_{wav}$ to $\overline{\eta}$ (respectively red and black curves in Fig. 3A–C) in the REF and LOWRES simulations. The storm surge event occurs during several hours from the 24th to the 26th of February with a maximum amplitude of ~1.0 m at the coast just south of L13 station. Despite differences between grid and resolution in both model settings, details in the simulated storm surge along the shoreline are quite similar. Fig. 3 highlights that the Gouaro channel area is less exposed to storm surge, which aligns with the 2D distribution shown in Fig. 4. In both REF and LOWRES (Fig. 3), storm surge >0.6 m are mainly concentrated to semi-enclosed bays (e.g "Baie des Tortues") or fringing reef zones (e.g "Plateau vidoire"). Importantly, both configurations show coastal storm surge peak (>0.8 m) along the whole Poe lagoon, where REF configuration captures a North/South asymmetry, whereas LOWRES displays a more uniform coastal distribution, which is consistent with Fig. 4. The main difference between REF and LOWRES simulations results in the storm surge duration. The prolonged storm surge (Fig. 3B and C) provides valuable insight into the event's duration and the lagoon's hydrodynamic response, including possible implications for lagoon flushing. Lasting 48 h in REF, it is shortened by half in LOWRES, indicating that the lagoon flushing may be more efficient in the low-resolution model grid configuration due to a possible drawback of unresolved details such as the exact openness of narrow channels, the submergence depth of the reef crest and the barrier reef geometry at lower resolution. Although the

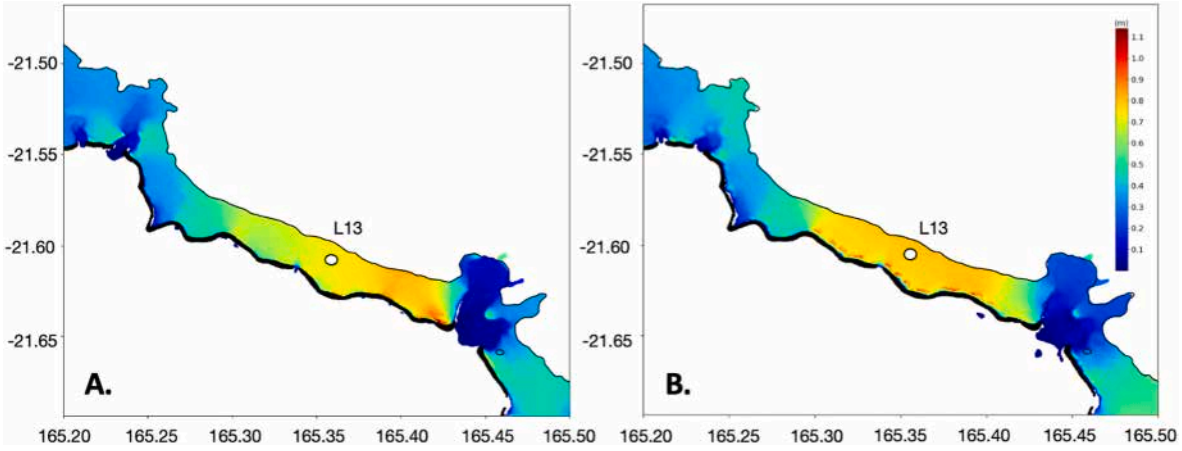

Fig. 4. Modeled maximum $\overline{\eta}_{wav}$ [m] during Oma TC (25th of February 2019) in Poe lagoon in REF (A) and LOWRES (B) configuration. The observation station L13 is located by the white point and the barrier reef with a black mask.

paper does not analyze detailed current dynamics, related processes are addressed in the idealized numerical experiments (see Section 3.3).

Over the whole measurement period, the observed storm surge can be primarily attributed to $\overline{\eta}_{wav}$ and especially during Oma TC, it accounted for more than 85 % of the storm surge in LOWRES and more than 95 % in REF (Fig. 3A–C). Since the wave breaking drives the storm surge, details on the spatial distribution of $\overline{\eta}_{wav}$ are provided in Fig. 4. Results reveal higher values of wave setup in the southern part of the lagoon, this asymmetry being more pronounced in REF than in LOWRES. In the REF configuration, the maximum of $\overline{\eta}_{wav}$ is concentrated in the southern section of the barrier reef, linked to a very shallow back reef (Fig. 4A), whereas in the LOWRES configuration, it is situated on both sides of the shark fault (Fig. 4B), related to a poorer representation of barrier reef details in LOWRES. It is worth noting that in the northern part of the lagoon, characterized with a more undulating reef, $\overline{\eta}_{wav}$ is reduced by half, with similar spatial patterns in both model settings.

3.3. Impact of the barrier reef geomorphology at the macro-scale on lagoon dynamics

To further understand factors controlling dynamics leading to the spatial pattern of $\overline{\eta}_{wav}$ shown in Fig. 4, the two idealized experiments, with a straight (IDEAL_S) and an undulating reef (IDEAL_W), are forced by stationary wave conditions corresponding to the peak of Oma (see Section 2.3.1 for details).

Fig. 5A illustrates the $\overline{\eta}_{wav}$ in the IDEAL_S configuration, showing a

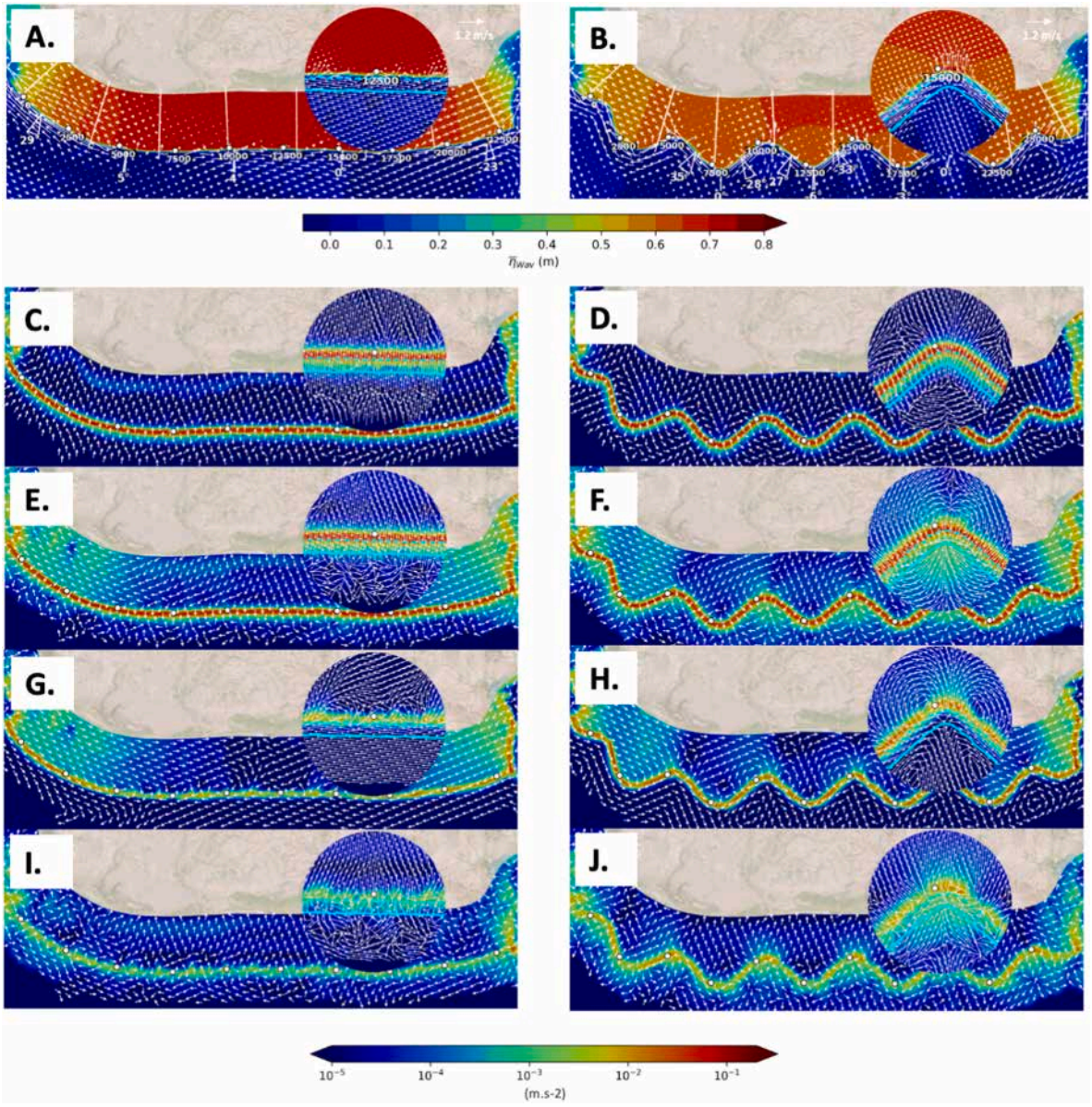

Fig. 5. Wave-driven circulation and leading terms of the momentum balance (Eq. (1)) at low tide under a stationary wave forcing with parameters corresponding to the peak of Oma TC (25th of February 2019) in two idealized reef-lagoon configurations: a straight reef (IDEAL_S, panel A) and a wavy barrier reef (IDEAL_W, panel B). (A, B) Simulated $\overline{\eta}_{wav}$ [m] and depth-averaged currents (white vectors), (C–D) wave force term, RSG, (E–F) barotropic pressure gradient term, PG, (G–H) bottom stress term, BF and (I–J) advective acceleration, ADV. The magnitude and direction of each term are represented by the map colors and the vectors respectively. Zooms are inserted in each panel to provide a detailed view across the barrier reef. White spots along the reef mark the position of the reef crest with ticks indicating the longshore length [m] of the reef crest at these positions. The shoaling zone is located between the shoaling line (solid line in cyan) at z~100 (=Lambda/2) and the breaking line (dashed line) at z~10m (= H_s/0.73), where the surf zone starts. The incidence angles (°) of breaking waves to the reef crest normal are indicated in white at a few locations. The white lines indicate examples of cross-shore lines where cross-shore integration of momentum terms is performed (see Fig. 12).

uniform response behind the reef crest and away from channels. The mean momentum balance (Eq. (1)) highlights $\overline{\eta}_{wav}$ as the result of an abrupt change in radiation stress gradient (RSG) from wave breaking, counterbalanced by the pressure gradient (PG) (Fig. 5C–E). In the shoaling zone delimited by the shoaling and breaking lines (see legend), on the forereef, RSG initially drives a slight setdown seaward, then reverses in the landward direction and peaks in the surf zone before sharply decreasing across the reef crest. PG dominates in the shoaling zones, while bottom friction (BF) contributes only marginally and remains confined to the reef flat (Fig. 5G). BF and advection (ADV), though small, indicate the presence of wave-driven across and along-reef currents (Fig. 5I). Within the channels, PG and BF balance as BF resists the lagoon water discharge driven by water level gradients. No significant circulation is observed in the central part of the lagoon, where depth-averaged currents remain negligible.

By contrast, in IDEAL_W configuration, $\overline{\eta}_{wav}$ is weaker and varies in the cross-shore and alongshore directions with the development of periodic current cells (Fig. 5B). RSG is still balance by PG on the reef face (Fig. 5D–F), but the effect of BF becomes important within the surf zone, with a magnitude one order larger than in IDEAL_S (Fig. 5H). ADV increases in the surf zone (Fig. 5J), a sign of more variability in the cross-reef transport along the reef, but in the shoaling zone too, as a sign of strong shear in flows. With a magnitude scaling with U^2, the increase in BF reveals the development of intense cross-reef currents, similar to rip currents (as mentioned in (Lowe et al., 2009)) at some places of the sine ribbon (e.g between distance ticks 13750 and 16250 on the reef line). Offshore, arrows in Fig. 5B describe well a convex coastline induced mega-rip circulation with an intense jet current oriented seaward. Unlike IDEAL_S, long-reef currents within the shoaling zone are intense, in places where the obliquity of wave with the reef increases (see values of θ sampled along the reef, Fig. 5B). The tuning of the waves during shoaling over the steep slope modifies a lot the magnitudes of the terms S_{xx}, S_{xy} and S_{yy} (see Eqs. (7)–(9)) strengthening wave-driven longshore currents and lowering $\overline{\eta}_{wav}$. Within gaps, PG displays a bulge owing to the convergence of along reef currents, fueling the offshore rip current. Over the reef, the breaking of normal incident waves is more intense in the apex of gaps, enhancing $\overline{\eta}_{wav}$ in the surf zone and toward the shoreline, compared to reef portions concerned with wider breaking angles. In the backreef region, an along reef PG owing to variations in $\overline{\eta}_{wav}$ develops, driving periodic current cells signaled above.

These idealized experiments help us in understanding the pattern of $\overline{\eta}_{wav}$ simulated in the realistic simulation of the Poe lagoon (Fig. 4) during Oma TC. The stronger $\overline{\eta}_{wav}$ observed in the southern area is in line with a straighter reef and the weaker and variable $\overline{\eta}_{wav}$ in the northern part with a more undulating reef. This result highlights the straight coupling between $\overline{\eta}_{wav}$ and variations in RSG along the barrier reef.

3.4. Control of wave setup dynamic by details in bathymetry and reef crest geometry

Besides the reef shape, details in the reef-lagoon bathymetry are also hypothesized to impact its dynamics and the induced $\overline{\eta}_{wav}$. The simulated maximum $\overline{\eta}_{wav}$ with a less accurate bathymetry product (LOWBAT) during Oma TC, and its relative change from REF are presented in Fig. 6A–D. Difference in amplitude does not exceed ±5 cm at L13 station but differences are more variable elsewhere in the lagoon with change up to ±10 % between both configurations. The LOWBAT configuration simulates a slightly weaker $\overline{\eta}_{wav}$ (-5 %) in the southern part of the lagoon and slightly stronger (+5 %) $\overline{\eta}_{wav}$ in the northern part (Fig. 6D). Since the average difference between depths in both bathymetry products (LOWBAT and REF) is ~1 m, our results indicate that a depth error of ~1 m might cause an error of ~10 % in the prediction of $\overline{\eta}_{wav}$.

From previous works (Buckley et al., 2015; Blenkinsopp and Chaplin, 2008; Yao et al., 2017), there is a large body of evidence that h_r, the submergence depth over the reef crest, has a large control on both the transmission of wave energy and magnitude of $\overline{\eta}_{wav}$. Fig. 6B, C shows the simulated maximum $\overline{\eta}_{wav}$ during Oma TC for a uniform reef crest height of 1 m (CR100) and 0.05 m (CR005) with their relative change from REF detailed in Fig. 6E and F. As indicated in Table 2, last row, these reef settings have an average h_r of 1.97 m and 1.13 m respectively, compared to 1.44 m in REF. For example, by reducing h_r by 20 % in CR005 compared to REF, the annual mean wave setup increases by 15 % (not shown). In Fig. 6F, that reduction in h_r exacerbates $\overline{\eta}_{wav}$ by 30 % during the storm, and peaks up to 50 % in the northern part of the lagoon. On the other hand, making h_r deeper (+37 % compared to REF) reduces $\overline{\eta}_{wav}$ by 15 % (-25 % in the southern part of the lagoon, see Fig. 6E). Overall,

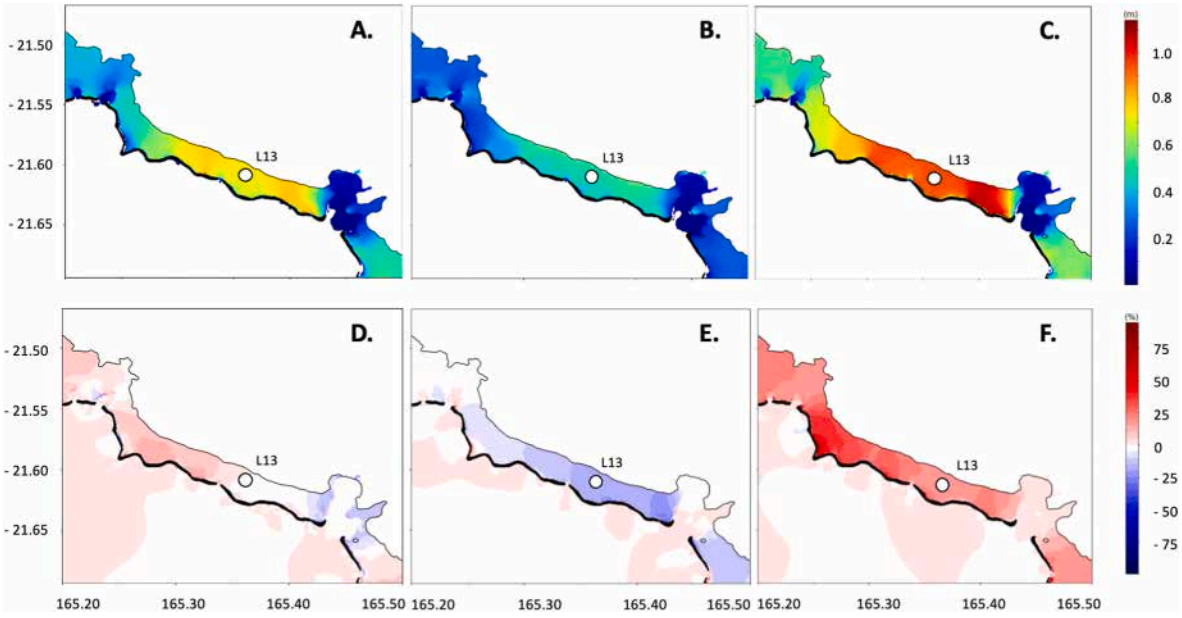

Fig. 6. Spatial distribution of maximum $\overline{\eta}_{wav}$ [m] during Oma TC (25th of February 2019) in Poe lagoon for the various model configurations used for sensitivity tests: a less accurate bathymetry product, LOWBAT (A), a homogeneous reef crest height set at 1.00 m, CR100 (B), and a uniform reef crest height set at 0.05 m, CR005 (C). The $\overline{\eta}_{wav}$ differences [%] are calculated by difference with REF for LOWBAT (D), CR100 (E) and CR005 (F). The observation station L13 is located by the white dot marker and the barrier reef is represented by a black mask.

Table 2
Transmission coefficient of H_s (k_t) between outside C02 station and inside L13 lagoon station for all experiments at low tide and high tide. Reef crest depth [m] in the model grid and submergence depth (h_r) above the reef crest [m] in both observations and models are given.

	OBS	REF	CR100	CR005	LOWRES
Transmission coefficient (k_t)					
Low tide	0.01 ± 0.01	0.25 ± 0.07	0.30 ± 0.09	0.23 ± 0.05	0.15 ± 0.05
High tide	0.13 ± 0.04	0.42 ± 0.12	0.47 ± 0.13	0.38 ± 0.10	0.22 ± 0.05
Barrier reef parameters					
Reef crest depth	X	1.0 to 1.35	1.0	0.05	0.7 to 1.3
Submergence depth over the reef crest (h_r)	0.80 (0.0–1.66)	1.44 (0.77–2.11)	1.97 (1.29–2.65)	1.13 (0.47–1.80)	1.36 (0.55–1.93)

our results indicate that the prediction of $\overline{\eta}_{wav}$ in a narrow lagoon, such as Poe lagoon, is very sensitive to details on the reef crest height. Moreover, rougher is the sea, the larger is the sensitivity of $\overline{\eta}_{wav}$ to the quality of h_r.

3.5. Prediction of the wave setup

A large bunch of work is devoted to derive $\overline{\eta}_{wav}$ using simple analytical predictive models based on sea state proxies (Guza and Thornton, 1981). derived the following relation for the wave setup as $\overline{\eta}_{wav} = 0.17H_s$, but other authors developed sophisticated relationships to account for the reef geomorphology (Gourlay, 1996). Such a relationship is investigated through observed and modeled $\overline{\eta}_{wav}$ and incident wave conditions (H_s) at station C02. Before fitting an empirical model, a data screening is applied, motivated by the theoretical works of (Gourlay, 1996) for wave setup on a fringing (closed lagoon) and platform reef (open lagoon) from laboratory experiments. It showed that the wave setup dynamics can be partitioned in two regimes, as indicated by a ratio between h_r and H_s, the relative submergence depth $S = \frac{(\overline{\eta}+h_r)}{H_s}$. The first regime, when S is large ($S > 0.7$ for open lagoons, or $S > 1.0$ for fringing reefs), describes cases where the water depth above the reef is relatively large compared to the incoming waves, driving a weak $\overline{\eta}_{wav}$, while the second regime, when S is small ($S < 0.7$ for open lagoons or $S < 1.0$ for fringing reefs), characterizes a relatively small water depth compared to incident waves, driving significant $\overline{\eta}_{wav}$ owing to wave breaking on the seaward reef-face. Such a metric is investigated in our dataset, indicating that 34 % of the observations fall in the first regime, generating low values of wave setup (not shown). Those observations are removed in the model to predict $\overline{\eta}_{wav} = f(H_s, h_r)$ at L13 station. The fitting curve with the 95 % prediction interval is displayed in Fig. 7A, providing a functional relational ($r^2 > 0.9$) which can serve later to compare with model results. For example, despite its lower resolution, the NC_BOX grid was shown to allow a reliable representation of storm surge compared to the REF higher resolution configuration (see Section 3.1) and here LOWRES is consistent with the slope of empirical law derived from observations (Fig. 7B). Fig. 7 also highlights an asymmetry between observed and modeled extreme values, though based on a single TC on limited monitoring period. Underestimation likely stems from biases in global wave products, as also reported by (Gaffet et al., 2025). This underscore increased bias in global wave models under cyclonic conditions and supports using a statistical approach to broaden TC case coverage.

3.6. Generalization of storm surge pattern under various TC forcings in Poe lagoon

In the following, we explore the generalization of the storm surge including IBE, wind stress and $\overline{\eta}_{wav}$ responses to extreme sea conditions by using STATTC and STATTC_NOWAVE configurations over the NC_BOX grid.

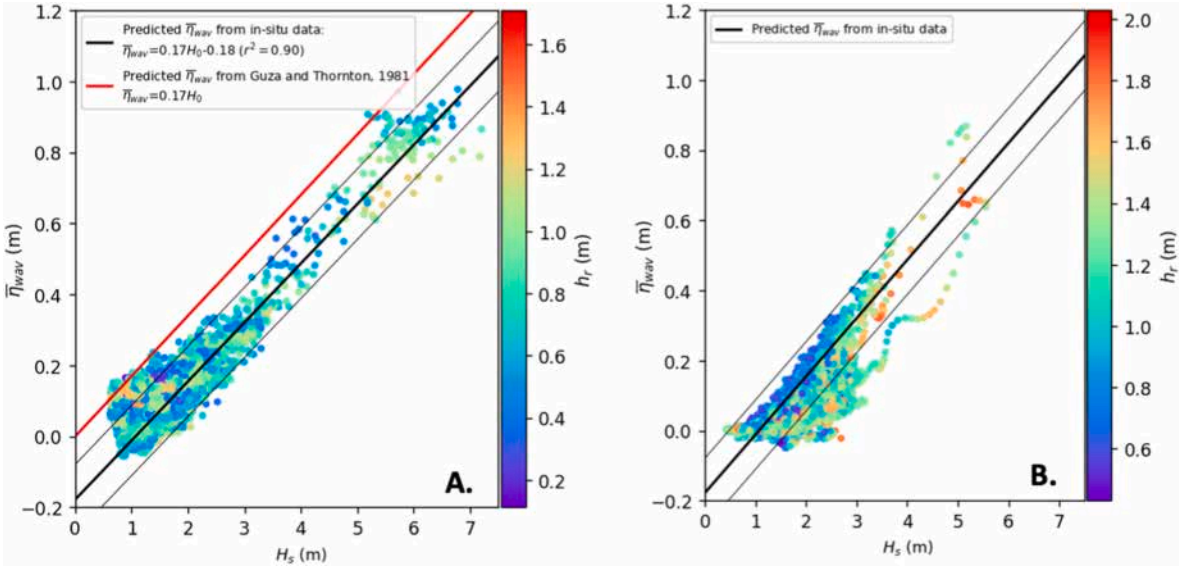

Fig. 7. Observed (panel A) and modeled (panel B) $\overline{\eta}_{wav}$ [m] at the lagoon station L13 for the period from 5th of February to 5th of May 2019 as a function of incident H_s [m] at station C02. Colors indicate the submergence depth above the reef crest noted h_r. Predicted $\overline{\eta}_{wav}$ following the relation of Guza and Thornton (1981) is indicated with the red line. The linear fit of $\overline{\eta}_{wav}$ with incident H_s from observations is indicated with the bold black line on both panels. The 95 % prediction intervals depicted with thin black lines and the associated regression coefficient (r^2) is indicated in the legend.

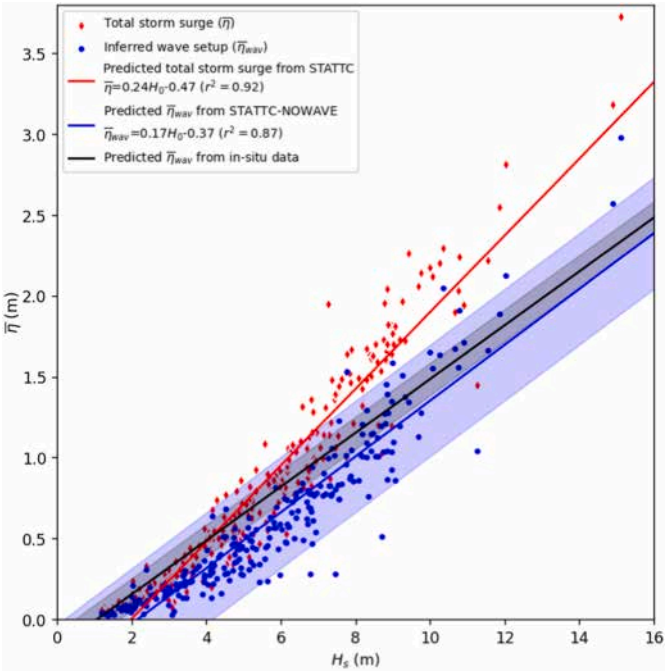

Fig. 8. Simulated storm surge including change in air pressure, wind stress (in red) and inferred $\overline{\eta}_{wav}$ (in blue) at station L13 [m] versus the deep-water wave heights H_s [m]. Curves from the linear fits for each variable are also displayed. The fitting of $\overline{\eta} = f(H_s)$ performed from STATTC outputs gives a slope of 0.24 m/m (r^2 = 0.92, red curve), while the fitting of $\overline{\eta}_{wav} = f(H_s)$ with $\overline{\eta}_{wav}$ from differences between STATTC and STATTC_NOWAVE outputs, gives a slope of 0.17 m/m (r^2 = 0.87, blue curve). The in-situ predictive model (see Fig. 7) for $\overline{\eta}_{wav}$ (black line) is indicated for comparison.

First, the quality of the storm surge generalization is investigated using our predictive model $\overline{\eta}_{wav} = f(H_s)$ developed in Section 3.5. Despite notable differences between the two scrutinized populations, one coming from a 5-months long monitoring, the other by targeting extreme storms in various TC conditions, Fig. 8 shows that simulated $\overline{\eta}_{wav}$ follow loosely the line of prediction (compare the blue curve with the black one). Also, we provide the result of the linear regression of $\overline{\eta}$ against H_s (see the red curve). With a slope of 0.17 m/m and 0.24 m/m respectively, this result indicates that $\overline{\eta}_{wav}$ is contributing 70 % for the superelevation of the mean water level at station L13. The falling of air pressure, wind stress and non-linear processes are involved to explain the remainder.

The generalized spatial pattern of the TC-induced storm surge and the relative wave contribution in percentage are illustrated for three statistics of the storm surge distribution: mean (Fig. 9A, B, C), 95th percentile (Fig. 9D, E, F) and maximum (Fig. 9G, H, I). In the open-ocean, the rise in water level ranges from 10 cm (Fig. 9A) to 80 cm (Fig. 9G), with a response driven by changes in air pressure (lowest pressure at the storm's center in the dataset is 924 hPa, resulting in an IBE of ~80 cm). Within the narrow lagoon, storm surges are in contrast much higher, with a large part explained by $\overline{\eta}_{wav}$ (above 65 % along the coastline and up 90 % in the surf zone, Fig. 9C–I). The lagoon mean storm surge peak exceeds 90 cm (against 10 cm offshore), the 95th percentile peaks at 2.0 m and the maximum exceeds 4.0 m (against 80 cm offshore). Details in the spatial pattern of $\overline{\eta}_{wav}$ tied to the lagoon dynamics resemble those investigated in Section 3.3 and Fig. 5. Unlike in the case of Oma TC, our statistical assessment reveals that, toward the shoreline, the prevailing contribution of $\overline{\eta}_{wav}$ vanishes a few as both the wind stress and the decrease of air pressure exacerbate the coastal storm surge. It is worth noting that in large embayments free of reef protection such as facing Gouaro, the breaking of swell on the beach contributes by half to the storm surge.

3.7. The impact of wave-induced hazards on coastal vulnerability

Fig. 9 indicate that extreme surge dynamics in complex reef settings induce a contrasted response in terms of coastal hazards. Fig. 10 shows the statistical distribution of incident wave height and storm surge values at 12 coastal locations. Fig. 10A, B are used to demonstrate the

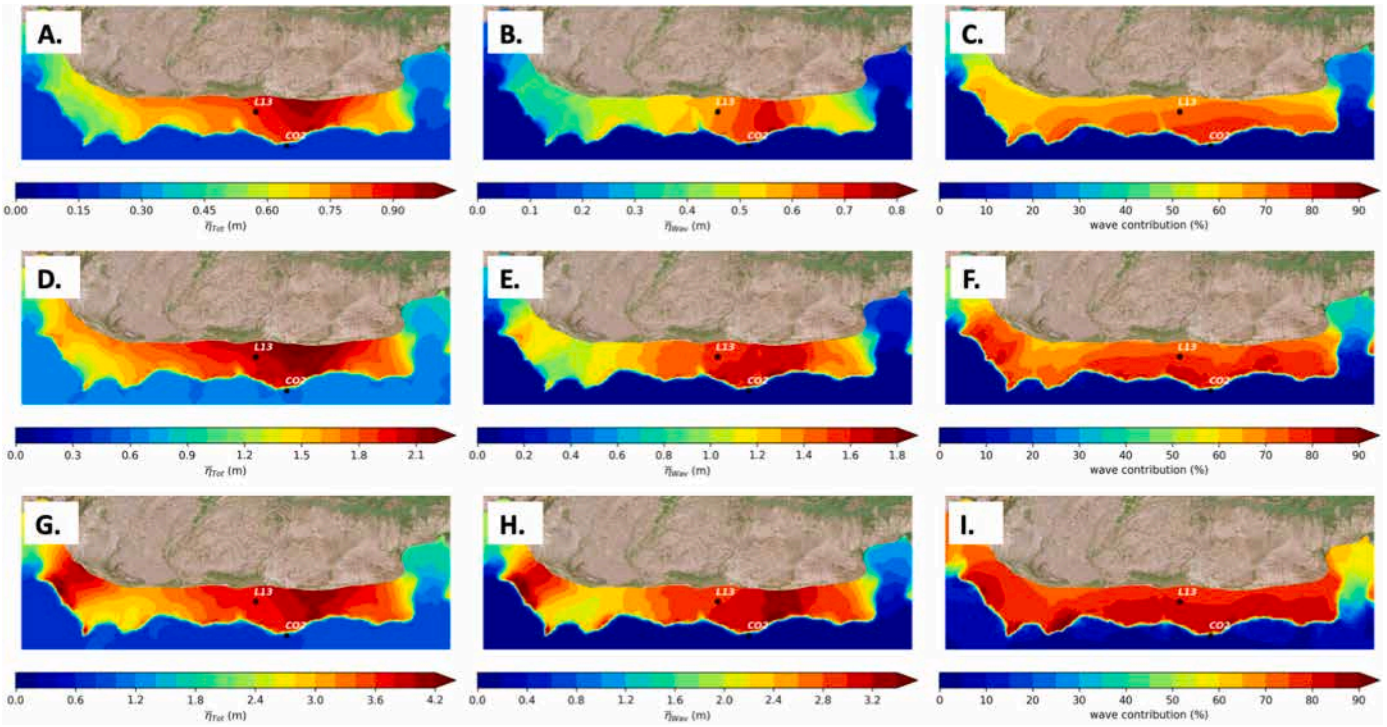

Fig. 9. Mean (A), 95th percentile (D) and maximum (G) storm surge [m] in Poe lagoon for 258 TC simulations (STATTC). Associated $\overline{\eta}_{wav}$ (panels B, E, H) [m] and its contribution [%] to storm surge (panels C, F, I) are calculated by the difference between STATTC and STATTC_NOWAVE simulations.

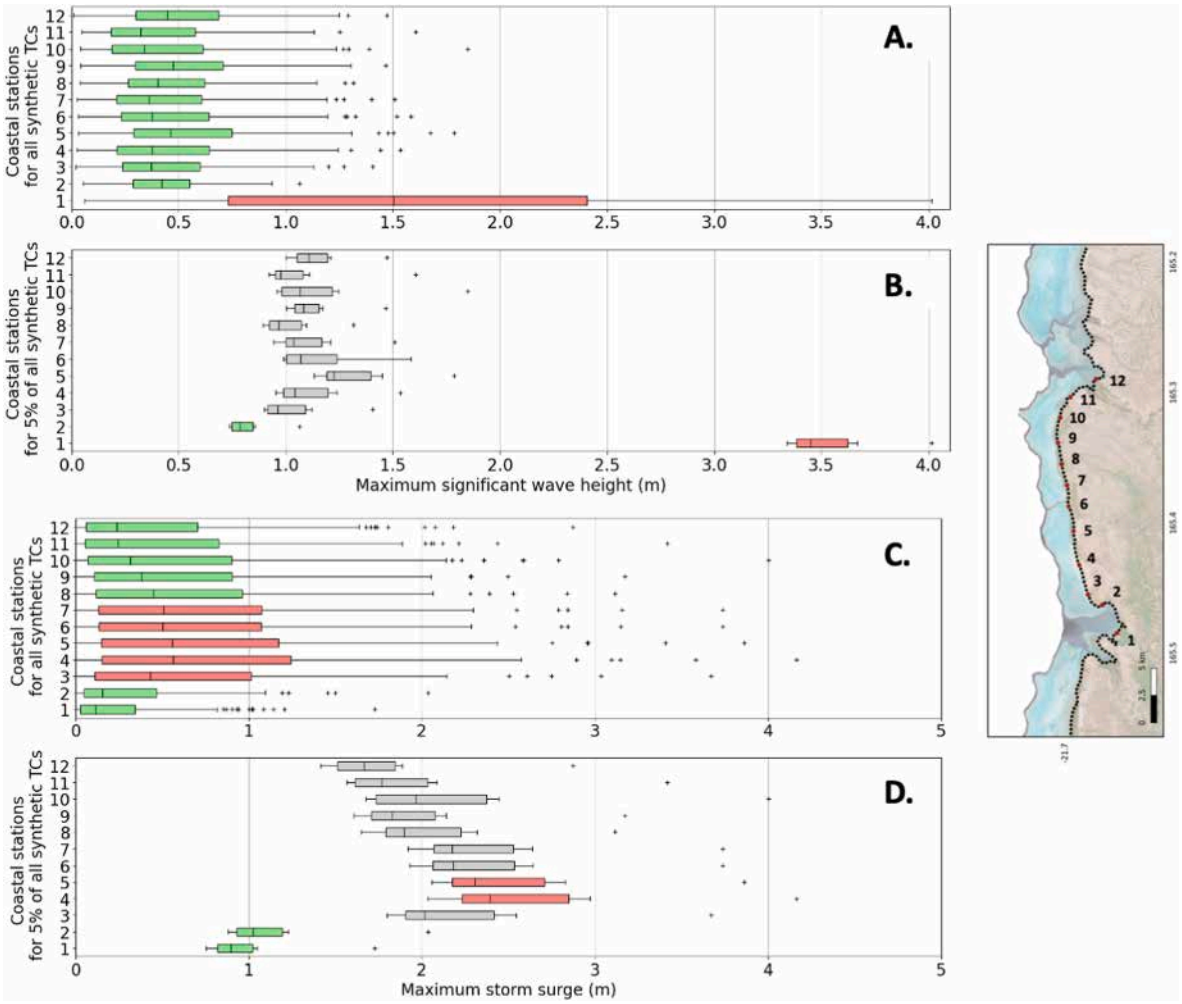

Fig. 10. Coastal H_s (panels A and B) and coastal storm surge (panels C and D) [m], for 12 virtual location along the coastline represented in the right panel. The whole distribution for the 258 synthetic TCs is represented in panels A and C, while only the 95th percentile of the events is represented in panels B and D. Colored bars denote the upper to lower quartiles, the black line denotes the median, the error bars denote the 1–99 percentiles and dots the most extreme events of the distribution. Colors provide a visual appreciation of the least (in green) to worst (in red) threatened locations.

mitigating role of the barrier reef to incident extreme TC waves and Fig. 10C, D shows the coastal storm surge.

Only station 1 (located at La Roche village, facing Gouaro) is directly exposed to extreme incident waves. There, at the coast, H_s values in the range 1.5–4.0 m account for over half of events (Fig. 10A), while waves above 3.3 m are reported in the tail of the TC distribution (above 95 %, Fig. 10B). These findings are consistent with (Storlazzi et al., 2022), who highlighted that localized bathymetric features such as channels can strongly influence coastal wave energy transmission. For the other coastal locations, half of events do not generate more than 50 cm waves, while in the 5 % more threatening events, H_s is capped at ~1.2 m. This result highlights that both the barrier reef and wave dissipation in the lagoon help to mitigate the height of destructive waves, preventing the aggravation of coastal flooding by overtopping. It is worth noting that within the southern lagoon, at location 5 in front of the Poe village, where many numerous habitations and human facilities are located, H_s are slightly higher, as a consequence of less dissipation by friction and breaking due to the increase of water depth with the wave setup as mentioned before.

On the other hand, storm surge strongly impacts locations in the lagoon away from the channels. From location 3 to 7, half of events induce a storm surge of at least 50 cm (Fig. 10C), while locations close to the channels (e.g 1 to 2 and 8 to 12), are less exposed to this hazard. Similar spatial features along the coastline are reported in the 5 % strongest storm surges, but locations 4 and 5 are the most exposed with storm surge greater than 2.0 m (Fig. 10D).

Changes in the coastal distribution of storm surges and coastal wave heights confirms a variable exposure to storm-induced hazards for that reef-lagoon setting. Here, overflowing may be associated with storm surge, while overtopping may arise due to individual wave incursion. Fig. 11 illustrates that double exposure along the coastline, which is partitioned in two distinct land use based on anthropic activities: the inhabited southern zone (sectors 1 to 4, Fig. 11), and the undeveloped northern zone (sectors 5 to 7, Fig. 11), which is free of constructions. Following the method from (Thomas et al., 2021) a populated area is assigned to each coastal sector, with a metric expressing the fraction of anthropic land use (Fig. 11). The area of La Roche village is urbanized up to 77 % (sector 1, Fig. 11) and is less concerned by storm surge as other sectors, but more exposed by extreme incident H_s due to its location facing the Gouaro channel. The touristic resort and Poe village urbanized up to 71 % and 78 % respectively (sectors 3 and 4, Fig. 11) are protected from incident H_s by the barrier reef but they are subjected to the highest storm surges mainly driven by $\overline{\eta}_{wav}$. Free of significant urban development at present, the other sectors (from 5 to 7, Fig. 11) appear

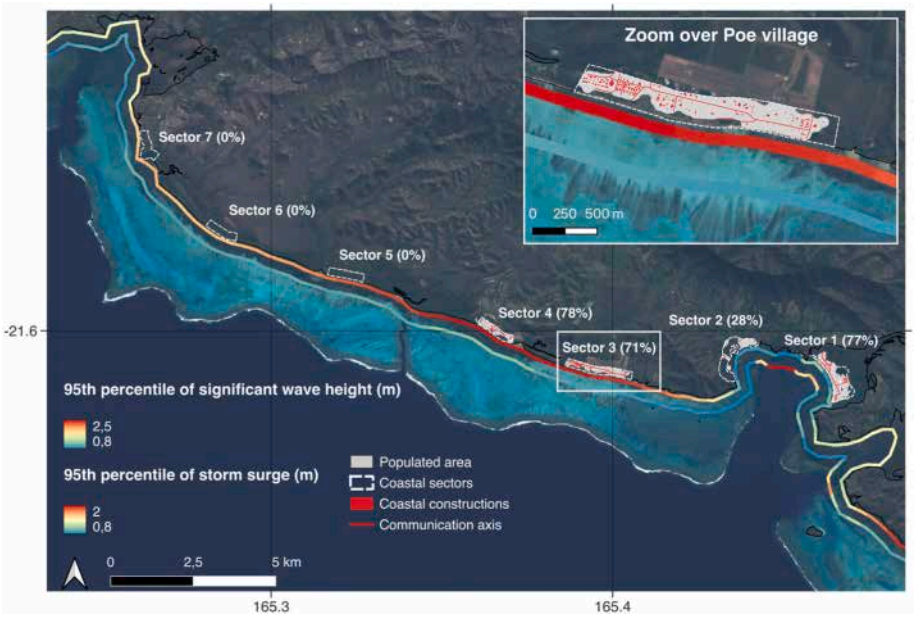

Fig. 11. Coastal exposure to H_s and storm surge, depicted by their respective 95th percentile [m] in Poe lagoon and associated zoom over urban areas such as Poe village. Urban density [%] is derived from populated areas including constructions and roads which is indicated for each coastal sector from 1 to 7. Populated areas are a proxy for population density based on land use.

less vulnerable since they are exposed to lower storm surge. In the light of this coastal hazards analysis, coastal management plans should consider limiting the urban development of the strongly threatened areas from sectors 1 to 4.

4. Discussion

4.1. Limitations of the modeling framework

While our modeling system has been shown to satisfactorily represent the observed offshore H_s and lagoon $\overline{\eta}_{wav}$, several limitations and sources of uncertainty can be discussed. A first notable point is that the simulated lagoon H_s is overestimated due to a too weak wave attenuation by the barrier reef. This is illustrated by evaluating the transmission coefficient of H_s through the reef, noted k_t with $k_t = \frac{H_s(L13)}{H_s(C02)}$ (see Table 2), which is much larger in REF and LOWRES model experiments (0.15–0.42) than in the observations (0.01–0.13). The submergence depth h_r is known to have a great influence on wave dissipation and wave setup prediction, but reducing h_r in CR005 by 30 % result in little improvement in k_t and has adverse effect on the storm surge by increasing a lot $\overline{\eta}_{wav}$. This suggests that efforts in tuning SWAN wave model to match the observed k_t across the barrier reef may be detrimental to the accuracy of $\overline{\eta}_{wav}$ predictions, recurrent evidence in studies applying linear wave theory in steep reef configurations as discussed in (Buckley et al., 2015; Sous et al., 2019).

This result is also pointing out the quality of the bottom stress parameterization, which controls the momentum sink term (Eq. (1)). It relies on a bottom drag coefficient, C_d, which is estimated using a log-layer treatment with a chosen bottom roughness and accounting for the presence of the wave boundary layer (Zhang et al., 2004). Coral reefs generate resistance to the water flow, however, the relationship between coral-induced friction and hydrodynamic roughness effects on waves and currents remains poorly understood (Lentz et al., 2017). In our simulations, we use a bottom roughness of 3 mm, leading to C_d values of ~0.01 on the forereef and backreef, and doubles above the shallow reef crest (not shown). Usually adapted to sandy seafloor (https://ccrm.vims.edu/schismweb/SCHISM_v5.6-Manual.pdf), that choice for z0 is questionable when representing coral reefs (Rosman and Hench, 2011). When compared with field studies in coral environments (Sous et al., 2020a), our simulated values are in the lower range of the observed values (from 0.01 to 0.3). To study the effect of bottom roughness on the prediction of $\overline{\eta}_{wav}$ and k_t in Poe (Martins et al., 2022; Guérin et al., 2018), a future dedicated 3D modeling study is considered.

Lastly, other important processes impacting coastal flooding are not resolved in our modeling strategy, such as the generation of infra-gravity waves owing to wave breaking and swash generated by waves (Pomeroy et al., 2012; Locatelli et al., 2017; Bertin et al., 2018). Their combination has the potential to increase the predicted runup (Aucan et al., 2017). Exploring these aspects however require dedicated studies with non-hydrostatic and phase-resolving wave models, as well as an accurate mapping of the reef crest by topo-bathymetric surveys (Collins et al., 2020).

4.2. Modulation of the wave setup due to change in water levels

A large body of works have shown that $\overline{\eta}_{wav}$ and the induced flow are strongly linked to variation in incident wave height (H_s), with a control by the water depth (h_r) due to tides (Monismith et al., 2013; Gourlay, 1996; Vetter et al., 2010). We claimed that, due to rough sea state, but moderate wind and weak air pressure drop during monitoring, and a data treatment designed to remove the tide variability, outputs from Eq. (2) make possible to derive $\overline{\eta}_{wav}$ and investigate $\overline{\eta}_{wav} = f(H_s, h_r)$ at station L13. But, one striking point from Fig. 7A is the lack of change in $\overline{\eta}_{wav}$ due to changes in the water depth. First, a limited observation time in that reef setting, concerned by transient piling-up, may make it difficult to demonstrate the tide modulation. Second, in contrast with past surveys

(Sous et al., 2020a; Vetter et al., 2010) using bottom pressure sensors on the reef flat, the station L13 is located in the back-reef lagoon, away from the surf zone. As indicated in Section 3.3, the wave-driven dynamics is complex there, and combined with the tide-driven dynamics, may hide that expected response.

To help in conclude and inspired by similar works (Lavaud et al., 2020) on the water level control of $\overline{\eta}_{wav}$, stationary outputs at low tide (LT) and high tide (HT) from the idealized numerical settings are recycled. Our results for IDEAL_S show that the shoreline $\overline{\eta}_{wav}$ is larger by 33 % at LT compared to HT (not shown). This is 31 % by doing the same experiment on the IDEAL_W. This indicates that the observed time serie does not include enough long-lasting surge events to help in isolating a robust tidal modulation of $\overline{\eta}_{wav}$.

4.3. The relevance of empirical laws and 1D models for estimating cyclonic surge hazard

While our empirical model based on incident wave conditions perform well at L13, its broader applicability to the whole lagoon is disputable as a consequence of large alongshore $\overline{\eta}_{wav}$ variability tied to the complex geomorphology. Moreover, our empirical relation agrees with Guza and Thornston's model, initially developed for a natural beach. When compared with a fringing-reef in Guam island (Vetter et al., 2010), with no back lagoon and channels, the predicted superelevation due to wave breaking at L13 is reduced by half in comparison (coefficient of determination above 0.30 m/m against 0.17 m/m here). In terms of coastal hazards, the shallow reef-lined coast of Poe is more relevant with a reef-lagoon-channel than a fringing reef, for which analytical models grounded on the 1D mass and momentum balanced equation (Eq. (1)) can be developed (Lowe et al., 2009; Gourlay, 1996). However, deriving such an 1D model might be a challenge, having regard to the impacts of macro scale details of the reef on the wave-driven circulation.

4.4. Predicting wave setup using the 1D momentum balance and insights

For a reef-lined coast (IDEAL_S, Fig. 5A), the wave incidence Θ where waves start breaking denoted (Θ_b) is controlled by depth contours along the reef due to wave refraction. In that setting, time averaged Θ_b are within 4° relative to the reef normal, also aligned with the shore normal. Owing to the small wave angle (Θ_b ~0), the cross-shore RSG term dominates Eq. (1), while $\frac{\partial S_{xy}}{\partial_y}$, the alongshore component vanishes, supporting its removal from Eq. (1). Integrating the cross-shore momentum balance (Eq. (1)) from the shoaling line (z = 100m) shoreward along each shore normal (see white line, Fig. 5A) is a mean to infer $\overline{\eta}_{wav}$ along the shoreline based on the mean momentum balance (Sous et al., 2020a; Rijnsdorp et al., 2021), while the cross-shore integral of each term in the right-hand side of Eq. (1) can provide their respective contribution in the balance of $\overline{\eta}_{wav}$. As shown in Fig. 12, the reconstructed wave setup is well in agreement with the simulated $\overline{\eta}_{wav}$ (compare the dotted black curve with the solid one, Fig. 12A), and results show that, in that ideal setting, reconstructing coastal $\overline{\eta}_{wav}$ only based on RSG is acceptable.

In an undulating setting (IDEAL_W, Fig. 5E), conditions to derive $\overline{\eta}_{wav}$ using the mean 1D momentum balance are violated, as a consequence of large variation in geometry and depths in the alongshore direction. However, integrating terms of Eq. (1) shoreward gives some useful information. Indeed, from Fig. 12B, both RSG and BF terms are needed to reconstruct accurately $\overline{\eta}_{wav}$ at the shoreline. Large variations in cross-integrals of BF is the manifestation of along reef changes in the net transport across the reef as discussed *in* Section 3.3. However, stopping the cross-integration of Eq. (1) after the reef flat implies to consider also ADV in order to give an accurate reconstruction of $\overline{\eta}_{wav}$ along the backreef line, for example (not shown). There, along-reef variations in $\overline{\eta}_{wav}$ of about 5–10 cm manifest since the curvature of the reef modifies both the wave height (compare the increase in the incident wave energy, the red curve, in Fig. 12A and B) and the angle at which the waves break. Non-negligible variations in gradients of the radiation stress terms S_{xy} and S_{yy} (Eqs. (8) and (9)) both in the shoaling and surfing zone, generate intense along-reef currents offshore and an along-reef pressure gradient owing to change in $\overline{\eta}_{wav}$ promoting a complicated wave-driven lagoon circulation. The result is a lowering of $\overline{\eta}_{wav}$ along the coastline (compare black solid curves, in Fig. 12A and B), as signaled in the real case between the southern and northern parts of Poe lagoon. Interestingly, peaks in the incident wave energy is another feedback owing to refraction with the mega-rip current directed offshore and grounded to the curved reef barrier. It is worth noting, that, switching off the current refraction in our modeling system, do not modify a lot $\overline{\eta}_{wav}$ both inferred from the cross-shore integrals or from model outputs (not shown), indicating that in such reef-lagoon setting, the wave-driven circulation and coastal $\overline{\eta}_{wav}$ is more sensitive to alongshore variation in wave direction than subtle variations in wave energy. A closer inspection

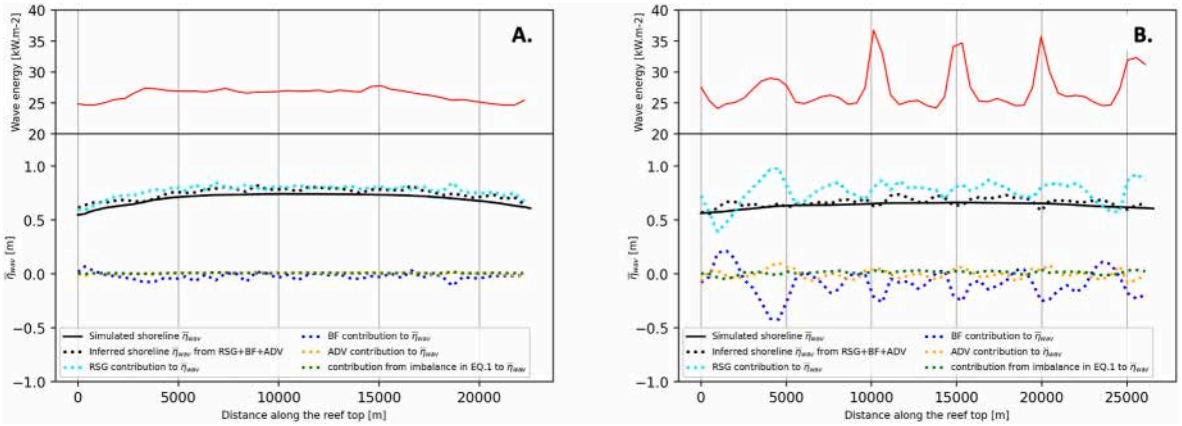

Fig. 12. Simulated and inferred $\overline{\eta}_{wav}$ along the shoreline for (A) the IDEAL_S and (B) IDEAL_W settings. The black solid line is $\overline{\eta}_{wav}$ from the 2D model outputs at the coast and the dashed black line is $\overline{\eta}_{wav}$ reconstructed using all mean cross-shore momentum terms from the 1D model (Eq. (1)), that is: RSG, BF and ADV. The contribution of RSG (cyan), BF (blue) and ADV (orange) to the reconstructed $\overline{\eta}_{wav}$ come from the cross-shore integrals of each term starting from the shoaling line (z~100m) up the coastline and by following normal transects spaced every 20 m in the alongshore direction (see cross-shore transects as those exemplified in Fig. 5). The green doted curve is the mean residual from imbalances of Eq. (1) showing their weak contribution to the reconstructed $\overline{\eta}_{wav}$. Along-reef variations of the wave energy forcing ($E = \frac{1}{8}\rho g {H_0}^2$) is illustrated by red solid curves and is extracted from SWAN outputs along the breaking line.

indicates that it is not BF but the ADV term that plays a key role in compensating along-reef variations in the RSG term imposed by switching off the current refraction (not shown).

4.5. Climate change induced coral reef trajectories for Poe lagoon

To strengthen the climate change perspective of the study, we conducted a REF simulation using a projected sea-level rise of +73 cm by 2100 for New Caledonia (SSP3-7.0 scenario). Results indicate a significant reduction in $\overline{\eta}_{wav}$ by 20–30 % under elevated sea levels in the southern sector of Poe lagoon and up to 60 % locally in the north. This reduction supports previous findings that higher sea levels reduce wave breaking over the reef crest, thereby weakening $\overline{\eta}_{wav}$ within the lagoon. However, sea-level rise also increases H_s by 20 % on average inside the lagoon and up to 40 % nearshore.

The coastal protection function of coral reefs is highly influenced by their elevation relative to mean sea level (Kench et al., 2022). However, the impact of projected sea-level rise on lagoon systems bounded by submerged barrier reefs remains insufficiently understood (Perry et al., 2018). This study emphasizes the crucial role of a healthy barrier reef (as documented by the non-profit association Paladalik, https://www.paladalik.com) in controlling wave setup and storm surge in Poe lagoon. In the face of rising sea-level, the capacity of coral communities to adapt remains an open challenge that requires extensive interdisciplinary research.

Under this scenario, the barrier reef persists with maintained ecological integrity and biological vitality. Numerous studies (Harris et al., 2018) underscore the importance of coral health and structural complexity for sustaining natural coastal protection into the future. Historical records show that some reefs have kept pace with sea-level changes on geological timescales (Camoin and Webster, 2015). Recent observations by (Kench et al., 2022) indicate that reef growth rates can reach 6.6 ± 12.5 mm/year on reef crests and 3.1 ± 10.2 mm/year on outer reef flats. These values exceed New Caledonia rates of sea-level rise, 2.23 ± 1.68 mm/year (Aucan et al., 2017) suggesting that healthy coral systems have the potential to maintain their mitigating function. The UNESCO-listed Poe lagoon is part of a broader marine protected area, which promotes the implementation of conservation policies that encompass coral reefs. Nevertheless, the coral reef remains exposed to local anthropic pressures, such as boating and fishing, and global threats including ocean warming and acidification. While these factors threaten reef adaptation capacity, nature-based solutions are gaining traction (Toth et al., 2023). propose that large-scale coral restoration could enhance reef accretion, potentially narrowing the elevation gap between reef tops and rising sea levels by 2100. Yet, the effectiveness of such strategies starts on an understanding of lagoon-scale hydrodynamics and wave processes as investigated in our study.

This scenario reflects a more degraded coral reef state, where barrier reef ability to provide coastal protection is significantly reduced. Accelerated environmental changes are degrading coral reefs and leading to the loss of species that significantly impacted wave energy dissipation (Carlot et al., 2023). As sea levels rise, the transmission of wave energy across reef platforms is expected to increase, reducing the natural buffering capacity of reef-lagoon systems (Costa et al., 2016). This effect is often accompanied by increases in significant wave height, potentially triggering secondary morphodynamical responses such as dune folding (Tuck et al., 2019). Poe lagoon is backed by an extensive sandy beach system, which plays a key role in coastal protection. However, in the absence of a functional reef barrier, these beach systems may become increasingly vulnerable. Future research should prioritize understanding beach dynamics and sediment redistribution processes, as highlighted by (Masselink et al., 2020), to evaluate the long-term sustainability of natural coastal buffers under barrier reef-degradation scenarios.

5. Conclusion

This study investigates the dynamics involved in the coastal storm surge in Poe, a reef-lagoon system using both observations and a wave-current coupled modeling system. The coastal hazard is then addressed through a generalization mobilizing two hundred TC storms. In such a narrow and shallow reef-lagoon, we have shown that the spatial variability of $\overline{\eta}_{wav}$ along the ~20 km-long coastline firstly depends on the barrier reef geomorphology, triggering variations in dynamics of the wave-driven flow and wave setup from place to place.

In particular, the shape of the barrier reef is found to play a crucial role, with a straighter barrier reef resulting in stronger and more uniform $\overline{\eta}_{wav}$ lagoon response (as suspected in the southern part), while the presence of headlands and gaps is promoting the generation of circulation loops and mega-rip currents offshore, lowering $\overline{\eta}_{wav}$ along the coast. Here, because of variations in the radiation stress gradient owing to change in the bathymetry and reef orientation, it is tricky to predict $\overline{\eta}_{wav}$ using empirical or semi-analytical formulations. For example, after tuning, a 1D model neglecting alongshore variations in the reef shape might be well adapted for a coast-lined reef, but might overestimate by 20 % the wave setup when applied to a more undulating reef setting.

In line with literature, h_r has also be shown to have significant influence on the induced $\overline{\eta}_{wav}$, with variations of ±1 m above the reef crest leading to a ±15–20 % change in $\overline{\eta}_{wav}$ within the lagoon. On the other hand, details in bathymetry within the lagoon is shown to have less influence on the accuracy of wave setup, with varying water depth of ±1 m on average in the lagoon resulting in only a ± 5–10 % change in $\overline{\eta}_{wav}$ in the southern area of the lagoon. We also tested a simple relationship linking offshore conditions to $\overline{\eta}_{wav}$ under extreme wind and wave events. Our $\overline{\eta}_{wav}$ estimates (70–90 %) align with previous studies (Lowe et al., 2009; Rijnsdorp et al., 2021; Vetter et al., 2010; Hsiao et al., 2019) which report contributions ranging from 50 % to over 80 % during similar high energetic conditions. Nevertheless, our results fall at the upper end of $\overline{\eta}_{wav}$ contributions to storm surge, emphasizing the need to systematically account for it when assessing storm impacts in reef-lagoon systems like Poe.

The analysis of 258 synthetic TC scenarios confirms patterns consistent with those observed during Oma. The southern sector of the lagoon, near the touristic area, is the most vulnerable to storm surge, while the highest wave exposure is concentrated off the Gouaro and La Roche village. Statistically, Poe village exhibits a high risk of cyclone-induced storm surge, with water levels exceeding 2 m at the 95th percentile, which is double the values studied in (Chen et al., 2017; Yu et al., 2019). These findings underscore the need to integrate such statistical hazard assessments into coastal management strategies in New Caledonia and other cyclone-prone regions.

Although global studies on reef protection (Burke and Spalding, 2022) and extreme sea-level hazards (Almar et al., 2021) offer valuable perspectives, they often lack the spatial resolution required to inform local-scale planning in lagoon environments. A logical next step involves assessing flood-related coastal risks at lagoon-scale. This will require combining cyclone scenario outputs with vulnerability datasets such as population density and critical infrastructure while also accounting for terrestrial flooding. The LECZ, bordered by a drainage basin, includes inhabited areas that are particularly vulnerable to flash flooding (Terry et al., 2008; Cerbelaud et al., 2022). As such, comprehensive coastal risk

assessments must account for compound hazards that encompass both marine and fluvial processes.

CRediT authorship contribution statement

Maxime Duphil: Writing – original draft, Visualization, Validation, Methodology, Funding acquisition, Formal analysis, Data curation, Conceptualization. **Jérôme Lefèvre:** Writing – review & editing, Visualization, Software, Methodology, Formal analysis, Data curation. **Swen Jullien:** Writing – review & editing, Investigation. **Jean Roger:** Writing – review & editing, Investigation. **Pascal Dumas:** Supervision. **Romain Le Gendre:** Investigation, Data curation. **Jérôme Aucan:** Investigation. **Myriam Vendé-Leclerc:** Funding acquisition. **Martin Bénébig:** Resources. **Christophe Menkes:** Writing – review & editing, Supervision, Investigation, Conceptualization.

Funding sources

This work was supported by the LABEX Corail (AO2020 - École Pratique des Hautes Études - Institut de Recherche pour le Développement - Bourse doctorale RESICOF).

Declaration of competing interest

The authors declare that they have no known competing financial interests or personal relationships that could have appeared to influence the work reported in this paper.

Appendices A.

Information about lagoon depth and spatial extension of both bathymetric grids used in the numerical model.

Appendices B.

Information about atmospheric (air pressure and wind) and incident wave conditions during Oma TC in New Caledonia used to force the SCHISM-SWAN numerical model.

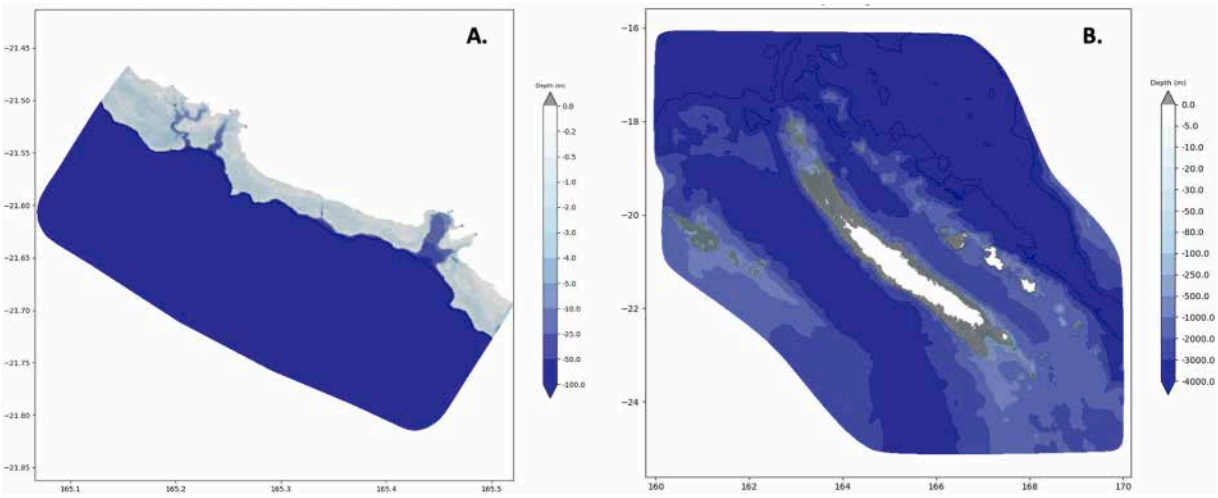

Fig. A1. Unstructured horizontal grids with bathymetry [m] for POE_BEACH (panel A) and NC_BOX (panel B) are performed with SHINGLE. It is particularly adapted to the complex structures of coral reefs as it is the case in Poe lagoon system.

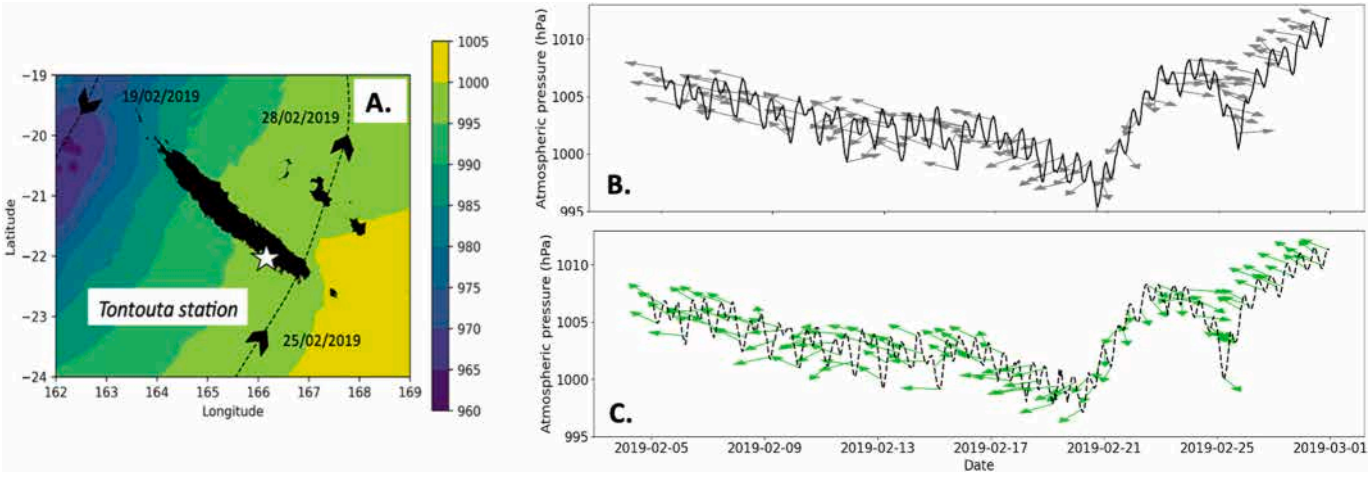

Fig. B1. The minimum atmospheric pressure (panel A) is calculated [hPa] on each grid node from AROME during February 2019. The Oma cyclone trajectory is indicated by a black dashed line with associated time. Time series of observed (grey arrows, panel B) and forced (green arrows, panel C) atmospheric pressure and wind direction during Oma cyclone in February 2019 at the Tontouta station (white star).

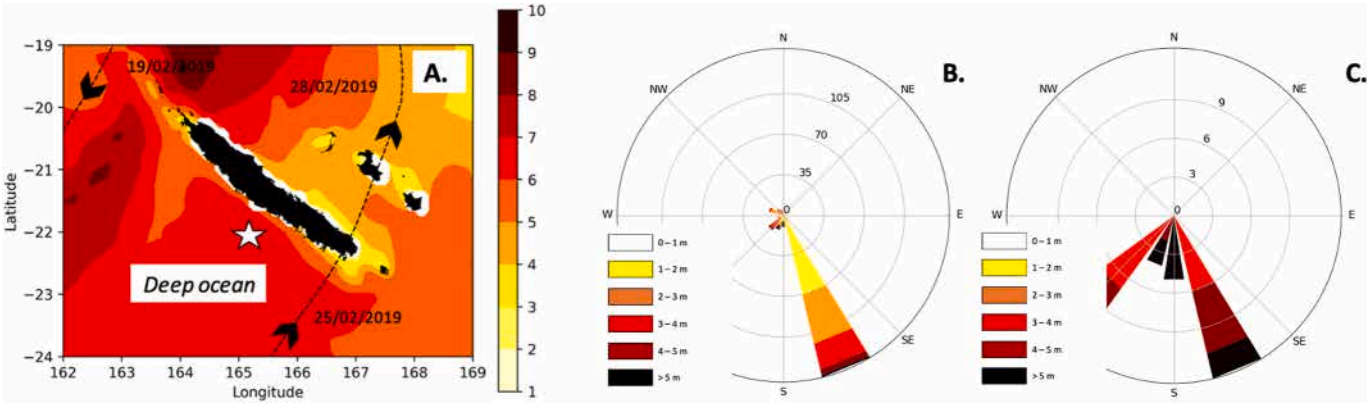

Fig. B2. The maximum significant wave height (panel A) is calculated [m] on each grid node from MFWAM during February 2019. The Oma cyclone trajectory is represented by a black dashed line with associated time. Wave roses of wave forcing from MFWAM during February 2019 (panel B) and during the cyclone peak in 48 h (panel C) at the deep ocean station (white star). The swell is mainly SSE during February, while during the cyclone, it is S-SW.

Data availability

Data will be made available on request.

References

Almar, R., Ranasinghe, R., Bergsma, E.W.J., Diaz, H., Melet, A., Papa, F., Vousdoukas, M., Athanasiou, P., Dada, O., Almeda, L.P., Kestenare, E., 2021. A global analysis of extreme coastal water levels with implications for potential coastal overtopping. Nat. Commun. 12, 3775. https://doi.org/10.1038/s41467-021-24008-9.

Amrari, S., Bourassin, E., Andrefouët, S., Soulard, B., Lemonnier, H., Le Gendre, R., 2021. Shallow water bathymetry retrieval using a band-optimization iterative approach: application to New Caledonia coral reef Lagoons using Sentinel-2 data. Remote Sens. 13, 4108. https://doi.org/10.3390/rs13204108.

Andrefouët, S., Wantiez, L., 2010. Characterizing the diversity of coral reef habitats and fish communities found in a UNESCO world heritage site: the strategy developed for Lagoons of New Caledonia. Mar. Pollut. Bull. 61, 612–620. https://doi.org/10.1016/j.marpolbul.2010.06.031.

Andrefouët, S., Muller-Karger, F.E., Robinson, J.A., Torres-Pulliza, D., Spraggins, S.A., Murch, B., 2006. Global assessment of modern coral reef extent and diversity for regional science and management applications: a view from space. Proceedings of 10th International Coral Reef Symposium, pp. 1732–1745.

Apotsos, A., Raubenheimer, B., Elgar, S., Guza, R., 2008a. Testing and calibrating parametric wave transformation models on natural beaches. Coast. Eng. 55, 224–235. https://doi.org/10.1016/j.coastaleng.2007.10.002.

Apotsos, A., Raubenheimer, B., Elgar, S., Guza, R., 2008b. Wave-driven setup and alongshore flows observed onshore of a submarine canyon. J. Geophys. Res. 113, C07025. https://doi.org/10.1029/2007JC004514.

Aucan, J., Vendé-Leclerc, M., Dumas, P., Bricquir, M., 2017. Wave forcing and morphological changes of New Caledonia lagoon islets: insights on their possible relations. C. R. Geosci. 349, 248–259. https://doi.org/10.1016/j.crte.2017.09.003.

Aucan, J., Desclaux, T., Le Gendre, R., Liao, V., Andréfouët, S., 2021. Tide and wave driven flow across the rim reef of the atoll of raroia (tuamotu, French Polynesia). Mar. Pollut. Bull. 171, 112718. https://doi.org/10.1016/j.marpolbul.2021.112718.

Barbier, E.B., Hacker, S.D., Kennedy, C., Koch, E.W., Stier, A.C., Silliman, B.R., 2011. The value of estuarine and coastal ecosystem services. Ecol. Monogr. 81, 169–193. https://doi.org/10.1890/10-1510.1.

Battjes, J., Janssen, J., 1978. Energy loss and Set-Up due to breaking of random waves. Coast. Eng. https://doi.org/10.1061/9780872621909.034.

Beck, M.W., Losada, I.J., Menendez, P., Reguero, B.G., Diaz-Simal, P., Fernandez, F., 2018. The global flood protection savings provided by coral reefs. Nat. Commun. 9, 2186. https://doi.org/10.1038/s41467-018-04568-z.

Becker, J.M., Merrifield, M.A., Ford, M., 2014. Water level effects on breaking wave setup for Pacific island fringing reefs: water level effects on wave setup. J. Geophys. Res. Oceans 119, 914–932. https://doi.org/10.1002/2013JC009373.

Bertin, X., Li, K., Roland, A., Zhang, Y.J., Breilh, J.F., Chaumillon, E., 2014. A modeling-based analysis of the flooding associated with Xynthia, central Bay of Biscay. Coast. Eng. 94, 80–89. https://doi.org/10.1016/j.coastaleng.2014.08.013.

Bertin, X., De Bakker, A., Van Dongeren, A., Coco, G., André, G., Ardhuin, F., Bonneton, P., Bouchette, F., Castelle, B., Crawford, W.C., Davidson, M., Deen, M., Dodet, G., Guérin, T., Inch, K., Leckler, F., McCall, R., Muller, H., Olabarrieta, M., Roelvink, D., Ruessink, G., Sous, D., Stutzmann, E., Tissier, M., 2018. Infragravity waves: from driving mechanisms to impacts. Earth Sci. Rev. 177, 774–799. https://doi.org/10.1016/j.earscirev.2018.01.002.

Bertin, X., Michaud, H., Pezerat, M., Aubry, A., Jeanson, M., 2025. Dynamics of infragravity waves across the Southern Reef barrier of Mayotte. Indian Ocean. Coastal Dynamics 2025. Aveiro, Portugal. https://hal.science/hal-04924854v1.

Blenkinsopp, C.E., Chaplin, J.R., 2008. The effect of relative crest submergence on wave breaking over submerged slopes. Coast. Eng. 55, 967–974. https://doi.org/10.1016/j.coastaleng.2008.03.004.

Bloemendaal, N., Haigh, I.D., De Moel, H., Muis, S., Haarsma, R.J., Aerts, J.C., 2020. Generation of a global synthetic tropical cyclone hazard dataset using STORM. Sci. Data 7, 40. https://doi.org/10.1038/s41597-020-0381-2.

Booij, N., Haagsma, I.J.G., Holthuijsen, L.H., Kieftenburg, A.T.M.M., Ris, R.C., Van Der Westhuysen, A.J., Zijlema, M., 2004. Swan Cycle III version 40.41. User's Manual 115p. https://swanmodel.sourceforge.io/download/zip/swanuse.pdf.

Bremer, L.L., Coffman, M., Summers, A., Kelley, L.C., Kinney, W., 2022. Managing for diverse coastal uses and values under sea level rise: perspectives from O'ahu, Hawai'i. Ocean Coast Manag. 225, 106151. https://doi.org/10.1016/j.ocecoaman.2022.106151.

Brisset, M., Van Wynsberge, S., Andrefouët, S., Payri, C., Soulard, B., Bourassin, E., Le Gendre, R., Coutures, E., 2021. Hindcast and near real-time monitoring of Green Macroalgae blooms in shallow coral Reef Lagoons using Sentinel-2: a new-caledonia case Study. Remote Sens. 13, 211. https://doi.org/10.3390/rs13020211.

Bruyère, O., Soulard, B., Lemonnier, H., Laugier, T., Hubert, M., Petton, S., Desclaux, T., Van Wynsberge, S., Le Tesson, E., Lefèvre, J., Dumas, F., Kayara, J.F., Bourassin, E., Lalau, N., Antypas, F., Le Gendre, R., 2022. Hydrodynamic and hydrological processes within a variety of coral reef lagoons: field observations during six cyclonic seasons in New Caledonia. Earth Syst. Sci. Data 14, 5439–5462. https://doi.org/10.5194/essd-14-5439-2022.

Buckley, M.L., Lowe, R.J., Hansen, J.E., Van Dongeren, A.R., 2015. Dynamics of wave setup over a steeply sloping fringing Reef. J. Phys. Oceanogr. 45, 3005–3023. https://doi.org/10.1175/JPO-D-15-0067.1.

Buckley, M.L., Lowe, R.J., Hansen, J.E., Van Dongeren, A.R., 2016. Wave setup over a fringing Reef with large bottom roughness. J. Phys. Oceanogr. 46, 2317–2333. https://doi.org/10.1175/JPO-D-15-0148.1.

Burke, L., Spalding, M., 2022. Shoreline protection by the world's coral reefs: mapping the benefits to people, assets, and infrastructure. Mar. Pol. 146, 105311. https://doi.org/10.1016/j.marpol.2022.105311.

Camoin, G.F., Webster, J.M., 2015. Coral reef response to Quaternary sea-level and environmental changes: state of the science. Sedimentology 62, 401–428. https://doi.org/10.1111/sed.12184.

Carlot, J., Vousdoukas, M., Rovere, A., Karambas, T., Lenihan, H.S., Kayal, M., Adjeroud, M., Pérez-Rosales, G., Hedouin, L., Parravicini, V., 2023. Coral reef structural complexity loss exposes coastlines to waves. Sci. Rep. 13, 1683. https://doi.org/10.1038/s41598-023-28945-x.

Cerbelaud, A., Lefèvre, J., Genthon, P., Menkes, C., 2022. Assessment of the WRF-Hydro uncoupled hydro-meteorological model on flashy watersheds of the Grande Terre tropical island of New Caledonia (South-West Pacific). J. Hydrol.: Reg. Stud. 40, 101003. https://doi.org/10.1016/j.ejrh.2022.101003.

Chaumillon, E., Bertin, X., Fortunato, A.B., Bajo, M., Schneider, J.L., Dezileau, L., Walsh, J.P., Michelot, A., Chauveau, E., Créach, A., Hénaff, A., Sauzeau, T., Waeles, B., Gervais, B., Jan, G., Baumann, J., Breilh, J.F., Pedreros, R., 2017. Storm-induced marine flooding: lessons from a multidisciplinary approach. Earth Sci. Rev. 165, 151–184. https://doi.org/10.1016/j.earscirev.2016.12.005.

Chen, W.-B., Lin, L.-Y., Jang, J.-H., Chang, C.-H., 2017. Simulation of typhoon-induced storm tides and wind waves for the Northeastern Coast of Taiwan using a tide–surge–wave coupled model. Water 9, 549. https://doi.org/10.3390/w9070549.

Collins, A., Brodie, K., Bak, A.S., Hesser, T., Farthing, M., Lee, J., Long, J., 2020. Bathymetric inversion and uncertainty estimation from synthetic surf-zone imagery with machine learning. Remote Sens. 12, 3364. https://doi.org/10.3390/rs12203364.

Costa, M.B.S.F., Araújo, M., Araújo, T.C.M., Siegle, E., 2016. Influence of reef geometry on wave attenuation on a Brazilian coral reef. Geomorphology 253, 318–327. https://doi.org/10.1016/j.geomorph.2015.11.001.

Cuttler, M.V.W., Hansen, J.E., Lowe, R.J., Drost, E.J.F., 2018. Response of a fringing reef coastline to the direct impact of a tropical cyclone. Limnol. Oceanogr. 3, 31–38. https://doi.org/10.1002/lol2.10067.

Diamond, H.J., Lorrey, A.M., Renwick, J.A., 2013. A Southwest Pacific tropical cyclone climatology and linkages to the El niño–southern oscillation. J. Clim. 26, 3–25. https://doi.org/10.1175/JCLI-D-12-00077.1.

Dietrich, J.C., Zijlema, M., Westerink, J.J., Holthuijsen, L.H., Dawson, C., Luettich, R.A., Jensen, R.E., Smith, J.M., Stelling, G.S., Stone, G.W., 2011. Modeling hurricane waves and storm surge using integrally-coupled, scalable computations. Coast. Eng. 58, 45–65. https://doi.org/10.1016/j.coastaleng.2010.08.001.

Dodet, G., Bertin, X., Bruneau, N., Fortunato, A.B., Nahon, A., Roland, A., 2013. Wave-current interactions in a wave-dominated tidal inlet. JGR Oceans 118, 1587–1605. https://doi.org/10.1002/jgrc.20146.

Duphil, M., 2024. Le rôle protecteur des écosystèmes (récifs et mangroves) face au risque de submersion côtière lors d'évènements extrêmes en Nouvelle Calédonie. Géophysique [Physics.geo-ph]. Sorbonne Université, Français. https://www.theses.fr/2024SORUS508.

Duvat, V.K.E., Magnan, A.K., 2019. Rapid human-driven undermining of atoll island capacity to adjust to ocean climate-related pressures. Sci. Rep. 9, 15129. https://doi.org/10.1038/s41598-019-51468-3.

Duvat, V.K.E., Magnan, A.K., Wise, R.M., Hay, J.E., Fazey, I., Hinkel, J., Stojanovic, T., Yamano, H., Ballu, V., 2017. Trajectories of exposure and vulnerability of small islands to climate change. WIREs Climate Change 8, e478. https://doi.org/10.1002/wcc.478.

Egbert, G.D., Erofeeva, S.Y., 2002. Efficient inverse modeling of Barotropic Ocean tides. J. Atmos. Oceanic Technol. 19, 183–204.

Faure, G., Chambon, P., Brousseau, P., 2020. Operational implementation of the AROME model in the tropics: Multiscale validation of rainfall forecasts. Weather Forecast. 35, 691–710. https://doi.org/10.1175/WAF-D-19-0204.1.

Ferrario, F., Beck, M.W., Storlazzi, C.D., Micheli, F., Shepard, C.C., Airoldi, L., 2014. The effectiveness of coral reefs for coastal hazard risk reduction and adaptation. Nat. Commun. 5, 3794. https://doi.org/10.1038/ncomms4794.

Ford, M., Merrifield, M.A., Becker, J.M., 2018. Inundation of a low-lying urban atoll island: Majuro, Marshall Islands. Nat. Hazards 91, 1273–1297. https://doi.org/10.1007/s11069-018-3183-5.

Gaffet, A., Bertin, X., Sous, D., Michaud, H., Roland, A., Cordier, E., 2025. A new global high-resolution wave model for the tropical ocean using WAVEWATCH III version 7.14. Geosci. Model Dev. 18, 1929–1946. https://doi.org/10.5194/gmd-18-1929-2025.

Gao, J., Luettich, R., Fleming, J., 2013. Development and initial evaluation of a generalized asymmetric tropical cyclone vortex model in ADCIRC. ADCIRC Users Group Meeting. US Army Corps of Engineers, Vicksburg, MS, USA.

Gourlay, M.R., 1996. Wave set-up on coral reefs. 1. Set-up and wave-generated flow on an idealised two-dimensional horizontal reef. Coast. Eng. 27, 161–193. https://doi.org/10.1016/0378-3839(96)00008-7.

Guannel, G., Arkema, K., Ruggiero, P., Verutes, G., 2016. The power of three: coral reefs, seagrasses and mangroves protect coastal regions and increase their resilience. PLoS One 11, e0158094. https://doi.org/10.1371/journal.pone.0158094.

Guérin, T., Bertin, X., Coulombier, T., De Bakker, A., 2018. Impacts of wave-induced circulation in the surf zone on wave setup. Ocean Model. 123, 86–97. https://doi.org/10.1016/j.ocemod.2018.01.006.

Guza, R.T., Thornton, E.B., 1981. Wave set-up on a natural beach. J. Geophys. Res. 86, 4133–4137. https://doi.org/10.1029/JC086iC05p04133.

Harris, D.L., Rovere, A., Casella, E., Power, H., Canavesio, R., Collin, A., Pomeroy, A., Webster, J.M., Parravicini, V., 2018. Coral reef structural complexity provides important coastal protection from waves under rising sea levels. Sci. Adv. 4, eaao4350. https://doi.org/10.1126/sciadv.aao4350.

Hasselmann, K., Barnett, T.P., Bouws, E., Carlson, H., Cartwright, D.E., Enke, K., Ewing, J.A., Gienapp, H., Hasselmann, D.E., Kruseman, P., Meerburg, A., Müller, P., Olbers, D.J., Richter, K., Sell, W., Walden, H., 1973. Measurements of wind-wave growth and swell decay during the joint North Sea wave Project (JONSWAP). Dtsch. Hydrogr. Z. A8 (12), 95–105.

Hoeke, R.K., McInnes, K.L., Kruger, J.C., McNeught, R.J., Hunter, J.R., Smithers, S.G., 2013. Widespread inundation of Pacific islands triggered by distant-source wind-waves. Global Planet. Change 108, 128–138. https://doi.org/10.1016/j.gloplacha.2013.06.006.

Hsiao, S.-C., Chen, H., Chen, W.-B., Chang, C.-H., Lin, L.-Y., 2019. Quantifying the contribution of nonlinear interactions to storm tide simulations during a super typhoon event. Ocean Engineering 194, 106661. https://doi.org/10.1016/j.oceaneng.2019.106661.

Huang, Z., Lenain, L., Melville, W.K., Middleton, J.H., Reineman, B., Statom, N., McCabe, R.M., 2012. Dissipation of wave energy and turbulence in a shallow coral reef lagoon. J. Geophys. Res. 117, 2011JC007202. https://doi.org/10.1029/2011JC007202.

Idier, D., Bertin, X., Thompson, P., Pickering, M.D., 2019. Interactions between mean Sea level, tide, surge, waves and flooding: mechanisms and contributions to Sea level variations at the Coast. Surv. Geophys. 40, 1603–1630. https://doi.org/10.1007/s10712-019-09549-5.

IPCC, Summary for Policymakers, 2021. In: Masson-Delmotte, V., Zhai, P., Pirani, A., Connors, S.L., Péan, C., Berger, S., Caud, N., Chen, Y., Goldfarb, L., Gomis, M.I., Huang, M., Leitzell, K., Lonnoy, E., Matthews, J.B.R., Maycock, T.K., Waterfield, T., Yelekçi, O., Yu, R., Zhou, B. (Eds.), Climate Change 2021: the Physical Science Basis. Contribution of Working Group I to the Sixth Assessment Report of the Intergovernmental Panel on Climate Change. Cambridge University Press. In Press.

Jullien, S., Aucan, J., Lefèvre, J., Peltier, A., Menkes, C.E., 2020. Tropical cyclone induced wave setup around New Caledonia during cyclone COOK (2017). J. Coast Res. 95, 1454. https://doi.org/10.2112/SI95-281.1.

Jullien, S., Aucan, J., Kestenare, E., Lengaigne, M., Menkes, C., 2024. Unveiling the global influence of tropical cyclones on extreme waves approaching coastal areas. Nat. Commun. 15, 6593. https://doi.org/10.1038/s41467-024-50929-2.

Kench, P.S., Beetham, E.P., Turner, T., Morgan, K.M., Owen, S.D., McLean, R.F., 2022. Sustained coral reef growth in the critical wave dissipation zone of a Maldivian atoll. Commun. Earth Environ. 3, 9. https://doi.org/10.1038/s43247-021-00338-w.

Klöck, C., Duvat, V.K.E., Nunn, P.D., 2022. Maladaptive diffusion? The spread of hard protection to adapt to coastal erosion and flooding along island coasts in the Pacific and Indian Ocean. Reg. Environ. Change 22, 136. https://doi.org/10.1007/s10113-022-01989-x.

Komen, G.J., Hasselmann, S., Hasselmann, K., 1984. On the existence of a fully developed windsea spectrum. J. Phys. Oceanogr. 14, 1271–1285.

Komen, G.J., Cavaleri, L., Donelan, M., Hasselmann, K., Hasselmann, S.P.A.E.M., 1994. Janssen. Dynamics and Modelling of Ocean Waves. Cambridge University Press, p. 532. https://doi.org/10.1017/CBO9780511628955.

Krien, Y., Testut, L., Islam, A.K.M.S., Bertin, X., Durand, F., Mayet, C., Tazkia, A.R., Becker, M., Calmant, S., Papa, F., Ballu, V., Shum, C.K., Khan, Z.H., 2017. Towards improved storm surge models in the northern Bay of Bengal. Cont. Shelf Res. 135, 58–73. https://doi.org/10.1016/j.csr.2017.01.014.

Krien, Y., Dudon, B., Roger, J., Arnaud, G., Zahibo, N., 2017b. Assessing storm surge hazard and impact of sea level rise in the Lesser Antilles case study of Martinique. Nat. Hazards Earth Syst. Sci. 17, 1559–1571. https://doi.org/10.5194/nhess-17-1559-2017.

Lalau, N., Van Wynsberge, S., Soulard, B., Petton, S., Le Gendre, R., 2022. A quick and cost-effective method for modelling water renewal in shallow coral reef lagoons. Coral Reefs 41, 1611–1626. https://doi.org/10.1007/s00338-022-02319-7.

Lavaud, L., Bertin, X., Martins, K., Arnaud, G., Bouin, M.-N., 2020. The contribution of short-wave breaking to storm surges: the case Klaus in the Southern Bay of Biscay. Ocean Model. 156, 101710. https://doi.org/10.1016/j.ocemod.2020.101710.

Lentz, S.J., Davis, K.A., Churchill, J.H., DeCarlo, T.M., 2017. Coral Reef drag coefficients – water depth dependence. J. Phys. Oceanogr. 47, 1061–1075. https://doi.org/10.1175/JPO-D-16-0248.1.

Li, G., Li, X., Yao, T., Che, T., Yang, H., Ma, M., Zhao, H., Pan, X., 2019. Heterogeneous sea-level rises along coastal zones and small islands. Science Bulletin 64, 748–755. https://doi.org/10.1016/j.scib.2019.04.023.

Locatelli, F., Sous, D., Rey, V., Chevalier, C., Bouchette, F., Touboul, J., Devenon, J.L., 2017. Wave transformation over the Ouano reef barrier, New Caledonia. Coastal Dynamics 13. https://doi.org/10.1016/j.csr.2019.07.010.

Longuet-Higgins, M.S., 1962. The directional spectrum of Ocean waves, and processes of wave generation. Proc. Roy. Soc. Lond. Math. Phys. Sci. 265, 286–315. No. 1322, A Discussion on Progress and Needs of Marine Science.

Lowe, R.J., Falter, J.L., Monismith, S.G., Atkinson, M.J., 2009. Wave-Driven circulation of a coastal reef–lagoon System. J. Phys. Oceanogr. 39, 873–893. https://doi.org/10.1175/2008JPO3958.1.

Madsen, O.S., 1994. Spectral wave-current bottom boundary layer flows. American Society of civil engineers. Coast. Eng. 384–398.

Mandlier, 2013. Field observations of wave refraction and propagation pathways on coral reef platforms. Earth Surf. Process. Landf. 913–925. https://doi.org/10.1002/esp.3328.

Martins, K., Bertin, X., Mengual, B., Pezerat, M., Lavaud, L., Guérin, T., Zhang, Y.J., 2022. Wave-induced mean currents and setup over barred and steep sandy beaches. Ocean Model. 179, 102110. https://doi.org/10.1016/j.ocemod.2022.102110.

Masselink, G., Beetham, E., Kench, P., 2020. Coral reef islands can accrete vertically in response to sea level rise. Sci. Adv. 6, eaay3656. https://doi.org/10.1126/sciadv.aay3656.

Monismith, S.G., Herdman, L.M.M., Ahmerkamp, S., Hench, J.L., 2013. Wave transformation and wave-driven flow across a steep coral Reef. J. Phys. Oceanogr. 43, 1356–1379. https://doi.org/10.1175/JPO-D-12-0164.1.

Nicholls, R.J., Cazenave, A., 2010. Sea-Level rise and its impact on coastal zones. Science 328, 1517–1520. https://doi.org/10.1126/science.1185782.

Pagli, B., Duphil, M., Jullien, S., Dutheil, C., Pelletier, A., Menkes, C., 2024. Wave climate around New Caledonia. Clim. Dyn. 62, 8865–8887. https://doi.org/10.1007/s00382-024-07365-1.

Pascal, N., Allenbach, M., Brathwaite, A., Burke, L., Le Port, G., Clua, E., 2016. Economic valuation of coral reef ecosystem service of coastal protection: a pragmatic approach. Ecosyst. Serv. 21, 72–80. https://doi.org/10.1016/j.ecoser.2016.07.005.

Patra, A., Min, S., Seong, M., 2020. Climate variability impacts on global extreme wave heights: seasonal assessment using satellite data and ERA5 reanalysis. JGR Oceans 125, e2020JC016754. https://doi.org/10.1029/2020JC016754.

Payri, C.E., Allain, V., Aucan, J., David, C., David, V., Dutheil, C., et al., 2019. Chapter 27 - new Caledonia. In: Sheppard, C. (Ed.), World Seas: an Environmental Evaluation, second ed. Academic Press, pp. 593–618. https://doi.org/10.1016/B978-0-08-100853-9.00035-X.

Pedreros, R., Idier, D., Muller, H., Lecacheux, S., Paris, F., Yates-Michelin, M., Dumas, F., Pineau-Guillou, L., Sénéchal, N., 2018. Relative contribution of wave setup to the storm surge: observations and modeling based analysis in open and protected environments (Truc vert beach and Tubuai Island). J. Coast Res. 85, 1046–1050. https://doi.org/10.2112/SI85-210.1.

Pelletier, D., 2024. Marine biodiversity in New Caledonia and contemporary conservation challenges. In: Kowasch, M., Batterbury, S.P.J. (Eds.), Geographies of New Caledonia-Kanaky. Springer. https://doi.org/10.1007/978-3-031-49140-5_4.

Perry, C.T., Alvarez-Filip, L., Graham, N.A.J., Mumby, P.J., Wilson, S.K., Kench, P.S., Manzello, D.P., Morgan, K.M., Slangen, A.B.A., Thomson, D.P., Januchowski, F.,

Smithers, S.G., Steneck, R.S., Carlton, R., Edinger, E.N., Enochs, I.C., Estrada-Saldivar, N., Haywood, M.D.E., Kolodziej, G., Murphy, G.N., Perez-Cervan, E., Suchley, A., Valentino, L., Boenish, R., Wilson, M., Macdonald, C., 2018. Loss of coral reef growth capacity to track future increases in sea level. Nature 558, 396–400. https://doi.org/10.1038/s41586-018-0194-z.

Pezerat, M., Bertin, X., Martins, K., Mengual, B., Hamm, L., 2021. Simulating storm waves in the nearshore area using spectral model: current issues and a pragmatic solution. Ocean Model. 158, 101737. https://doi.org/10.1016/j.ocemod.2020.101737.

Pomeroy, A., Lowe, R., Symonds, G., Van Dongeren, A., Moore, C., 2012. The dynamics of infragravity wave transformation over a fringing reef: infragravity waves over a fringing reef. J. Geophys. Res. https://doi.org/10.1029/2012JC008310.

Reguero, B.G., Storlazzi, C.D., Gibbs, A.E., Shope, J.B., Cole, A.D., Cumming, K.A., Beck, M.W., 2021. The value of US coral reefs for flood risk reduction. Nat. Sustain. 4, 688–698. https://doi.org/10.1038/s41893-021-00706-6.

Rijnsdorp, D.P., Buckley, M.L., Da Silva, R.F., Cuttler, M.V.W., Hansen, J.E., Lowe, R.J., Green, R.H., Storlazzi, C.D., 2021. A numerical Study of wave-driven mean flows and setup dynamics at a coral reef-lagoon System. J. Geophys. Res. Oceans. https://doi.org/10.1029/2020JC016811.

Roger, J., Pelletier, B., Aucan, J., 2019. Update of the tsunami catalogue of New Caledonia using a decision table based on seismic data and marigraphic records. Nat. Hazards Earth Syst. Sci. 19, 1471–1483. https://doi.org/10.5194/nhess-19-1471-2019.

Roger, J., Pelletier, B., Duphil, M., Lefèvre, J., Aucan, J., Lebellegard, P., Thomas, B., Bachelier, C., Varillon, D., 2021. The 7.5 Tadine (Maré, Loyalty Islands) earthquake and related tsunami of 5 December 2018: seismotectonic context and numerical modeling. Nat. Hazards Earth Syst. Sci. 21, 3489–3508. https://doi.org/10.5194/nhess-21-3489-2021.

Rosman, J.H., Hench, J.L., 2011. A framework for understanding drag parameterizations for coral reefs. J. Geophys. Res. 116, C08025. https://doi.org/10.1029/2010JC006892.

Snyder, R.L., Dobson, F.W., Elliott, J.A., Long, R.B., 1981. Array measurements of atmospheric pressure fluctuations above surface gravity waves. J. Fluid Mech. 102, 1–59. https://doi.org/10.1017/S0022112081002528.

Sous, D., Tissier, M., Rey, V., Touboul, J., Bouchette, F., Devenon, J.L., Chevalier, C., Aucan, J., 2019. Wave transformation over a barrier reef. Cont. Shelf Res. 184, 66–80. https://doi.org/10.1016/j.csr.2019.07.010.

Sous, D., Dodet, G., Bouchette, F., Tissier, M., 2020a. Momentum balance across a barrier Reef. J. Geophys. Res. Oceans 125. https://doi.org/10.1029/2019JC015503.

Sous, D., Bouchette, F., Doerflinger, E., Meulé, S., Certain, R., Toulemonde, G., Dubarbier, B., Salvat, B., 2020b. On the small-scale fractal geometrical structure of a living coral reef barrier. Earth Surf. Process. Landf. 45, 3042–3054. https://doi.org/10.1002/esp.4950.

Storlazzi, C.D., Ogston, A.S., Bothner, M.H., Field, M.E., Presto, M.K., 2004. Wave- and tidally-driven flow and sediment flux across a fringing coral reef: southern Molokai, Hawaii. Cont. Shelf Res. 24, 1397–1419. https://doi.org/10.1016/j.csr.2004.02.010.

Storlazzi, C.D., Gingerich, S.B., Van Dongeren, A., Cheriton, O.M., Swarzenski, P.W., Quataert, E., Voss, C.I., Field, D.W., Annamalai, H., Piniak, G.A., McCall, R., 2018. Most atolls will be uninhabitable by the mid-21st century because of sea-level rise exacerbating wave-driven flooding. Sci. Adv. 4, eaap9741. https://doi.org/10.1126/sciadv.aap9741.

Storlazzi, C.D., Rey, A.E., Van Dongeren, A.R., 2022. A numerical Study of geomorphic and oceanographic controls on wave-driven runup on fringing reefs with shore-normal channels. JMSE 10, 828. https://doi.org/10.3390/jmse10060828.

Symonds, G., Black, K.P., Young, I.R., 1995. Wave-driven flow over shallow reefs. J. Geophys. Res. 100 (C2), 2639–2648. https://doi.org/10.1029/94JC02736.

Taebi, S., Lowe, R.J., Pattiaratchi, C.B., Ivey, G.N., Symonds, G., 2012. A numerical study of the dynamics of the wave-driven circulation within a fringing reef system. Ocean Dyn. 62, 585–602. https://doi.org/10.1007/s10236-011-0514-4.

Terry, J.P., Kostaschuk, R.A., Wotling, G., 2008. Features of tropical cyclone-induced flood peaks on Grande Terre, New Caledonia. Water Environ. J. 22, 177–183. https://doi.org/10.1111/j.1747-6593.2007.00098.x.

Thomas, B.E.O., Roger, J., Gunnell, Y., Sabinot, C., Aucan, J., 2021. A low-cost toolbox for high-resolution vulnerability and hazard-perception mapping in view of tsunami risk mitigation: application to New Caledonia. Int. J. Disaster Risk Reduct., 102350 https://doi.org/10.1016/j.ijdrr.2021.102350.

Toth, L.T., Storlazzi, C.D., Kuffner, I.B., Quataert, E., Reyns, J., McCall, R., Stathakopoulos, A., Hillis-Starr, Z., Holloway, N.H., Ewen, K.A., Pollock, C.G., Code, T., Aronson, R.B., 2023. The potential for coral reef restoration to mitigate coastal flooding as sea levels rise. Nat. Commun. 14, 2313. https://doi.org/10.1038/s41467-023-37858-2.

Tuck, M.E., Ford, M.R., Masselink, G., Kench, P.S., 2019. Physical modelling of reef island topographic response to rising sea levels. Geomorphology 345, 106833. https://doi.org/10.1016/j.geomorph.2019.106833.

Van Dongeren, A., Lowe, R., Pomeroy, A., Trang, D.M., Roelvink, D., Symonds, G., Ranasinghe, R., 2013. Numerical modeling of low-frequency wave dynamics over a fringing coral reef. Coast. Eng. 73, 178–190. https://doi.org/10.1016/j.coastaleng.2012.11.004.

Vetter, O., Becker, J.M., Merrifield, M.A., Pequignet, A.C., Aucan, J., Boc, S.J., Pollock, C.E., 2010. Wave setup over a Pacific Island fringing reef. J. Geophys. Res. 115, 2010JC006455. https://doi.org/10.1029/2010JC006455.

Vitousek, S., Barnard, P.L., Fletcher, C.H., Frazer, N., Erikson, L., Storlazzi, C.D., 2017. Doubling of coastal flooding frequency within decades due to sea-level rise. Sci. Rep. 7, 1399. https://doi.org/10.1038/s41598-017-01362-7.

Yao, Y., He, W., Du, R., Jiang, C., 2017. Study on wave-induced setup over fringing reefs in the presence of a reef crest. Appl. Ocean Res. 66, 164–177. https://doi.org/10.1016/j.apor.2017.06.002.

Yao, Y., Huang, Z., He, W., Monismith, S.G., 2018. Wave-induced setup and wave-driven current over Quasi-2DH reef-lagoon-channel systems. Coast. Eng. 138, 113–125. https://doi.org/10.1016/j.coastaleng.2018.04.009.

Ye, F., Zhang, Y.J., Yu, H., Sun, W., Myers, E., Nunez, K., Zhang, R., Wang, H.V., Roland, A., Martins, K., Bertin, X., Du, J., Liu, Z., 2020. Simulating storm surge and compound flooding events with a creek-to-ocean model: importance of baroclinic effects. Ocean Model. 145, 101526. https://doi.org/10.1016/j.ocemod.2019.101526.

Yu, H.-C., Zhang, Y.J., Yu, J.C.S., Terng, C., Sun, W., Ye, F., Wang, H.V., Wang, Z., Huang, H., 2017. Simulating multi-scale oceanic processes around Taiwan on unstructured grids. Ocean Model. 119, 72–93. https://doi.org/10.1016/j.ocemod.2017.09.007.

Yu, Y.-C., Chen, H., Shih, H.J., Chang, C.H., Hsiao, S.C., Chen, W.B., Su, W.R., Lin, L.Y., 2019. Assessing the potential highest storm tide hazard in Taiwan based on 40-Year historical typhoon surge hindcasting. Atmosphere 10, 346. https://doi.org/10.3390/atmos10060346.

Zhang, H., Madsen, O.S., Sannasiraj, S.A., Soon Chan, E., 2004. Hydrodynamic model with wave–current interaction in coastal regions. Estuar. Coast Shelf Sci. 61, 317–324. https://doi.org/10.1016/j.ecss.2004.06.002.

Zhang, Y.J., Witter, R.C., Priest, G.R., 2011. Tsunami–tide interaction in 1964 Prince William Sound tsunami. Ocean Model. 40, 246–259. https://doi.org/10.1016/j.ocemod.2011.09.005.

Zhang, Y.J., Ye, F., Stanev, E.V., Grashorn, S., 2016. Seamless cross-scale modeling with SCHISM. Ocean Model. 102, 64–81. https://doi.org/10.1016/j.ocemod.2016.05.002.

Zhu, G., Ren, B., Lin, P., Dong, P., 2024. Numerical study of wave-induced flow and wave set-up on a platform reef with steep slope. Appl. Ocean Res. 148, 104030. https://doi.org/10.1016/j.apor.2024.104030.

Zijlema, M., 2010. Computation of wind-wave spectra in coastal waters with SWAN on unstructured grids. Coast. Eng. 57, 267–277. https://doi.org/10.1016/j.coastaleng.2009.10.011.

Zijlema, M., Van Vledder, G. Ph, Holthuijsen, L.H., 2012. Bottom friction and wind drag for wave models. Coast. Eng. 65, 19–26. https://doi.org/10.1016/j.coastaleng.2012.03.002.